PLANT SCIENCE TODAY
Vol 13(sp9): 01-12
https://doi.org/10.14719/pst.17031

eISSN 2348-1900
OPEN ACCESS

Review Article | Agriculture
2026, Volume 13, Issue sp9, pp. 01-31

Plant disease detection and recognition using hyperspectral remotely sensed data: A review

Vishalini Sivasubramani[1], Kumaraperumal Ramalingam[1*], Jagadeeswaran Ramasamy[1], Sivasubramanian Karuppusamy[2], Kavitha Shanmugam[3], Nivas Raj Moorthi[1] & Sai Divya Sri Jagarlamudi[1]

[1]Department of Remote Sensing and Geographic Information System, Tamil Nadu Agricultural University, Coimbatore 641 003, Tamil Nadu, India

[2]Department of Agronomy, Tamil Nadu Agricultural University, Coimbatore 641 003, Tamil Nadu, India

[3]Centre for Students Welfare, Tamil Nadu Agricultural University, Coimbatore 641 003, Tamil Nadu, India

***Correspondence:** Kumaraperumal Ramalingam, kumaraperumal.r@tnau.ac.in

Abstract

Plant diseases are an inevitable challenge in agricultural production, yet timely intervention and effective management practices can significantly prevent crop losses and sustain yield and quality. Conventional diagnostic approaches depend on visual evaluation and labour-intensive, time-consuming physical sample collection, making them inadequate for large-scale crop monitoring and often detecting diseases only after visible symptoms appear, considerably hampering the potential for early disease detection. These limitations necessitate unbiased and automated approaches to disease monitoring and diagnosis. By measuring spectral reflectance across hundreds of continuous wavelength bands in the visible, near-infrared (NIR) and shortwave infrared (SWIR) domains, hyperspectral remote sensing represents a revolutionary technique facilitating non-invasive, spatially comprehensive crop health assessment. Disease-related physiological and metabolic changes such as chlorophyll loss, water stress and pigment alteration generate distinctive spectral signatures detectable by hyperspectral sensors with high resolution. Hyperspectral data analysis employs spectral vegetation indices (VIs), feature selection and machine/deep learning models to enable automated, high-accuracy disease classification, substantially improving detection efficiency over conventional field scouting. However, the technology's practical deployment is constrained by high sensor costs, large data volumes, spectral redundancy, sensitivity to illumination and calibration variability and the scarcity of large, labelled datasets, which limit model generalisability across crops and environments. Combining hyperspectral data with other complementary remote sensing techniques through multisensor integration enhances the accuracy and spatial resolution of plant disease detection. This review elucidates hyperspectral data acquisition, preprocessing and analytical techniques for plant disease detection, current methodologies, applications and research gaps, positioning hyperspectral remote sensing as a foundational technology for next-generation sustainable agriculture.

Keywords: disease classification; dimensionality reduction; feature extraction; machine learning; spectral reflectance; vegetation indices

Received: 26 July 2026. **Accepted:** 16 September 2026. **Available online:** 16 November 2026.

Cite this article: Vishalini S, Kumaraperumal R, Jagadeeswaran R, Sivasubramanian K, Kavitha S, Nivas RM, Sai Divya SJ. Plant disease detection and recognition using hyperspectral remotely sensed data: A review. Plant Science Today. 2026;13(sp9):01-31. https://doi.org/10.14719/pst.17031

Introduction

Plant diseases pose an alarming threat to worldwide agricultural production and food security. The distribution, host range and consequences of plant diseases are increasing due to global climate change and the rapid expansion of international trade. Diseases that have already been controlled may re-emerge (1). To fulfil the increasing demand for both the quantity and quality of food, plant protection is necessary, particularly for preventing crops from diseases.

Nearly 10–40 % of global production is lost due to plant diseases. Detection and diagnosis of diseases have been accomplished using conventional techniques such as microscopy, culturing, immunoassays and molecular analyses, which are complicated, time-consuming and constrained to centralised laboratories. Most of these techniques suffer from low sensitivity and specificity and thus fail to combat emerging plant diseases. The existing techniques used for detection normally require the crop agronomist to conduct a visual inspection for symptoms that have appeared by physically examining the crop. Given the fact that many commercially grown crops cover a vast area, monitoring crop growth using this technique is highly labour-intensive. The manual detection of any diseases requires visible symptoms, which only appear when the disease is at an advanced stage. Highly sensitive, rapid and economical methods

of detecting and diagnosing plant diseases have become an urgent need. Recent developments in computer science and biotechnology have contributed to developing new technologies for disease detection. Among these, biological sensing and remote imaging methods appear to be the most promising ones (2, 3).

Plant disease detection has increasingly relied on non-invasive optical sensors such as hyperspectral imaging. The use of such technology is more accurate than traditional methods in both precision farming and resistance breeding and its applications range from laboratory testing to field studies. Specifically, hyperspectral imaging is important for the diagnosis of diseases as it offers advantages at various levels, starting from individual plant testing to canopy-level assessment (4).

Hyperspectral imaging (HSI) has become an important technique for precision agriculture applications compared to standard imaging methods that employ multispectral or visible spectrum (RGB) data. Hyperspectral imaging can identify plant stress, disease and nutritional deficiencies by examining each crop's distinct spectral signature. This information can be utilised to maximise crop productivity and lower input costs (5). By utilising machine learning (ML) methods and algorithms combined with hyperspectral images, diseases can be identified. A broad range of wavelengths can be observed in hyperspectral images. Cereals, oilseeds, fruits, vegetables and other agricultural crops can be monitored using these wavelengths, among other applications. Crop parameters such as nutritional status and maturity index, as well as the early identification of some diseases that result in crop losses, can be examined and diagnosed within these wavelength ranges (6).

Plant disease detection starts with image acquisition and is accompanied by segmentation-based pre-processing. This is further done in association with various methods of feature extraction as well as classification (7). Machine learning and deep learning algorithms are advancing the process of image classification-based disease identification using artificial intelligence (AI) (8). The aim of this review is to provide a comprehensive overview of the application of hyperspectral remotely sensed data for plant disease detection, covering several aspects of hyperspectral remote sensing such as sensing principles, sensors, spectral features, pre-processing methods, feature extraction techniques, vegetation indices (VIs) and ML methods. The following sections discuss these aspects in detail.

Materials and Methods

Plant diseases pose an alarming threat to worldwide agricultural production and food security. The distribution, host range and consequences of plant diseases are increasing due to global climate change and the rapid expansion of international trade. Diseases that have already been controlled may re-emerge (1). To fulfil the increasing demand for both the quantity and quality of food, plant protection is necessary, particularly for preventing crops from diseases.

Nearly 10–40 % of global production is lost due to plant diseases. Detection and diagnosis of diseases have been accomplished using conventional techniques such as microscopy, culturing, immunoassays and molecular analyses, which are complicated, time-consuming and constrained to centralised laboratories. Most of these techniques suffer from low sensitivity and specificity and thus fail to combat emerging plant diseases. The existing techniques used for detection normally require the crop agronomist to conduct a visual inspection for symptoms that have appeared by physically examining the crop. Given the fact that many commercially grown crops cover a vast area, monitoring crop growth using this technique is highly labour-intensive. The manual detection of any diseases requires visible symptoms, which only appear when the disease is at an advanced stage. Highly sensitive, rapid and economical methods of detecting and diagnosing plant diseases have become an urgent need. Recent developments in computer science and biotechnology have contributed to developing new technologies for disease detection. Among these, biological sensing and remote imaging methods appear to be the most promising ones (2, 3).

Plant disease detection has increasingly relied on non-invasive optical sensors such as hyperspectral imaging. The use of such technology is more accurate than traditional methods in both precision farming and resistance breeding and its applications range from laboratory testing to field studies. Specifically, hyperspectral imaging is important for the diagnosis of diseases as it offers advantages at various levels, starting from individual plant testing to canopy-level assessment (4).

Hyperspectral imaging (HSI) has become an important technique for precision agriculture applications compared to standard imaging methods that employ multispectral or visible spectrum (RGB) data. Hyperspectral imaging can identify plant stress, disease and nutritional deficiencies by examining each crop's distinct spectral signature. This information can be utilised to maximise crop productivity and lower input costs (5). By utilising ML methods and algorithms combined with hyperspectral images, diseases can be identified. A broad range of wavelengths can be observed in hyperspectral images. Cereals, oilseeds, fruits, vegetables and other agricultural crops can be monitored using these wavelengths, among other applications. Crop parameters such as nutritional status and maturity index, as well as the early identification of some diseases that result in crop losses, can be examined and diagnosed within these wavelength ranges (6).

© The Author(s) 2026. Creative Commons CC BY 4.0. Published by Horizon e-Publishing Group.
https://doi.org/10.14719/pst.17031

Plant disease detection starts with image acquisition and is accompanied by segmentation-based pre-processing. This is further done in association with various methods of feature extraction as well as classification (7). Machine learning and deep learning algorithms are advancing the process of image classification-based disease identification using artificial intelligence (AI) (8). The aim of this review is to provide a comprehensive overview of the application of hyperspectral remotely sensed data for plant disease detection, covering several aspects of hyperspectral remote sensing such as sensing principles, sensors, spectral features, pre-processing methods, feature extraction techniques, VIs and ML methods. The following sections discuss these aspects in detail.

Scope and methodology of this review

Literature search strategy

Taking into account the multi-stage pipeline of hyperspectral remote sensing for plant disease identification, the review has been structured around eight thematic strands spanning sensing, preprocessing, feature extraction, VIs, machine learning, deep learning, sensor integration and future prospects. The identification and organisation of these themes were based on the literature assessed through the various database searches conducted for this review.

Google Scholar, Scopus, Web of Science, Elicit and Institute of Electrical and Electronics Engineers (IEEE) Xplore were employed to obtain research on hyperspectral remote sensing applications for plant disease detection and recognition, spanning studies published from 2015–26. Google Scholar was used for broad multidisciplinary coverage across agriculture and remote sensing journals; Scopus was used for its extensive indexing of peer-reviewed journal articles across agricultural, remote sensing and computer science domains; Web of Science was used to ensure coverage of high-impact, citation-indexed research and to support backward citation tracing of foundational studies in the field; Elicit was used for AI-assisted semantic search and rapid screening of relevant studies across published research; and IEEE Xplore was used to capture engineering and sensor-focused literature on hyperspectral instrumentation and data-driven classification methods.

Search query

The literature search utilised keyword-based queries across the title, abstract and keywords fields, structured around the eight thematic pillars of this review:

Google scholar and elicit search queries

“Hyperspectral disease detection”; “preprocessing of hyperspectral data”; “feature extraction hyperspectral”; “VIs for disease detection”; “ML disease detection hyperspectral”; “deep learning disease detection hyperspectral”; “integration of remote sensing sensors plant disease”; “future scope hyperspectral plant disease detection”.

Institute of Electrical and Electronics Engineers Xplore search query

(“hyperspectral imaging” OR “hyperspectral remote sensing”) AND (“plant disease” OR “crop disease” OR “plant stress detection”) AND (“machine learning” OR “deep learning” OR “feature extraction” OR “preprocessing” OR “sensor fusion”).

Each keyword group was searched independently and, where relevant, combined (e.g., “hyperspectral” + “deep learning” + “disease detection”) to capture literature specific to each subsection of the review.

Study selection and screening

The preliminary search resulted in 163 papers, which were screened for relevance using the following criteria:

Inclusion criteria

- Research on hyperspectral (imaging or non-imaging) sensing for plant/crop disease or stress detection.
- Studies of spectral data employing machine learning, deep learning, feature extraction, or preprocessing techniques; empirical or review articles, peer-reviewed, published in English, from 2015 until 2026.

Exclusion criteria

- Duplicate or irrelevant studies.
- Studies based on only RGB or multispectral data without a hyperspectral component.
- Application studies for non-agricultural/plant diseases.

After screening, 100 articles were selected for in-depth review. Among them, 11 articles concern sensor types and data acquisition, including instruments for imaging and non-imaging hyperspectral collection; 16 articles address preprocessing and feature extraction methods; 18 articles address VIs and spectral signatures for disease detection; 30 articles address ML and deep learning classification/regression approaches; and 25 articles emphasise sensor fusion, integration with other remote sensing modalities and future prospects in precision agriculture. The article selection process followed the preferred reporting items for systematic reviews and meta-analyses (PRISMA) framework, as shown in Fig. 1.

Hyperspectral remote sensing

Remote sensing technologies fall into two categories: 1) passive (optical) and active (LiDAR and radar). The spectral resolution of the sensors used determines whether passive optical remote sensing is typically separated into two categories: multispectral and hyperspectral remote sensing. Among the methods of passive remote sensing that quantify reflected solar radiation or an artificial light source, hyperspectral sensing shows significant promise as a non-destructive, non-invasive method of monitoring biotic and abiotic plant stress (9).

© The Author(s) 2026. Creative Commons CC BY 4.0. Published by Horizon e-Publishing Group.
https://doi.org/10.14719/pst.17031

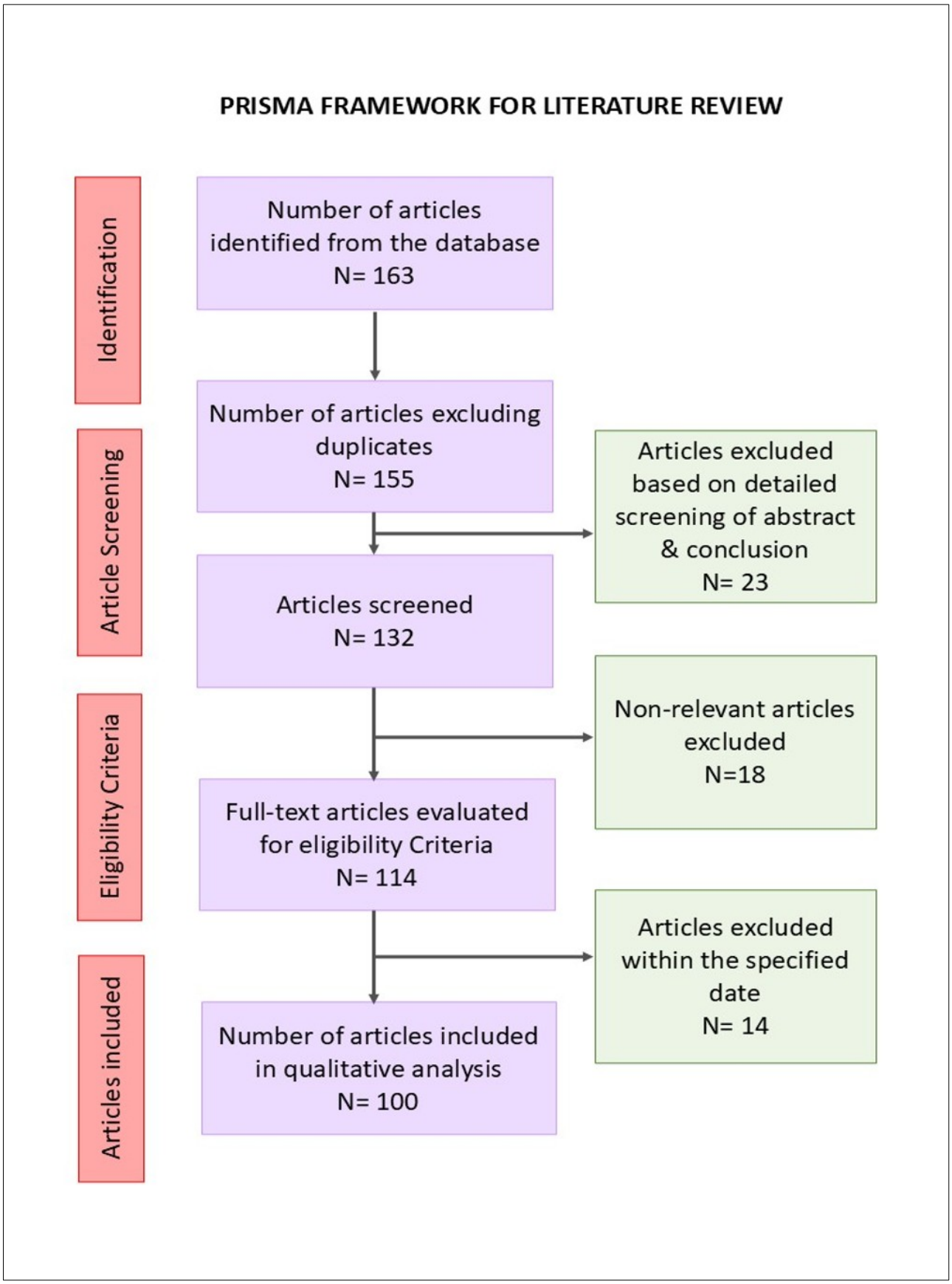


Fig. 1. PRISMA flowchart depicting the article selection process used in this review.

© The Author(s) 2026. Creative Commons CC BY 4.0. Published by Horizon e-Publishing Group.
https://doi.org/10.14719/pst.17031

By capturing hundreds of continuous spectral bands, hyperspectral remote sensing, also referred to as imaging spectroscopy, provides comprehensive spectral reflectance data of imaged targets.

Thousands of bands that represent various types of light energy make up the electromagnetic spectrum. Imaging spectrometers (instruments that capture hyperspectral data) divide the electromagnetic spectrum into groups of bands that assist in the classification of objects by their spectral qualities on the target's surface. Farmers can identify plant health issues and take preventative action before they become serious issues due to their capacity to record many wavelength bands and high-resolution images that provide adequate crop information (6).

Hyperspectral remote sensing employs a wide spectrum of wavelengths, spanning from the visible near-infrared (VNIR) to the shortwave infrared (SWIR) range of 400–2500 nm, facilitating a non-invasive approach to identify molecule reflection and absorption (10).

Hyperspectral images, comprising numerous narrow spectral bands, provide an accurate spectral reflectance curve capable of detecting minor changes in soil, canopies or individual leaves, facilitating the early identification of plant diseases through slight variations in spectral reflectance (9). In order to accurately and promptly determine the physiological status of agricultural crops, a broader range of problems can be solved using hyperspectral images. Timely detection of disease outbreaks and their spread may avoid significant agricultural losses, reduce pesticide application and mitigate their harmful impacts on the ecosystem and public health.

Hyperspectral versus multispectral imaging

Researchers have been using multispectral imagery (images including 3–20 discrete bands that are not contiguous) to identify diseases in crops for years. Because hyperspectral imaging can capture continuous spectral information spanning the visible, red edge and near-infrared (NIR) plateau regions, it has proven to be clearly superior to multispectral systems for the detection of crop diseases like wheat leaf rust. Hyperspectral systems may identify minute biochemical alterations in infected plant tissue before obvious symptoms appear, in contrast to multispectral sensors that are restricted to a few distinct wavebands (11).

By employing ML and deep learning approaches to process these images, they have discovered new findings that lead to more efficient analysis methodologies and save time (12). Despite this advantage, hyperspectral imaging is not always the best choice. Multispectral systems remain sufficient when the target disease produces distinct, well-characterised spectral signatures detectable within a few known bands, providing useful benefits in terms of cost, data volume, processing speed and compatibility with current satellite platforms (e.g., Sentinel-2, Landsat). Multispectral imaging is preferred for large-scale, time-sensitive, orcost-constrained monitoring where symptoms are already spectrally distinguishable, whereas hyperspectral imaging is most justified for early, asymptomatic infection stages or diseases with subtle biochemical signatures requiring fine spectral resolution (often <10 nm bandwidth).

Hyperspectral sensors and data acquisition

The initial and most critical step in analysing plant diseases is acquiring high-quality hyperspectral images. Achieving accurate results depends on selecting appropriate sensors and platforms, properly configuring spatial and spectral resolution, designing an effective lighting setup and correctly adjusting scan rate, frame rate and exposure time (13).

Three bands of the visual portion of the electromagnetic spectrum-red, green and blue light-are measured by conventional RGB cameras, while multispectral sensors measure the spectral information of objects across several discrete bands spanning the visible, NIR, red-edge and SWIR regions. Hyperspectral sensors capture several hundred bands in the electromagnetic spectrum (spectral range of 400–2500 nm and with a narrow spectral resolution of less than 1 nm). Each of these spectral bands only captures a few nanometres of the electromagnetic spectrum, so the hyperspectral sensor has a high spectral resolution. There are two types of sensors: imaging sensors and non-imaging sensors (14, 15).

Non-imaging sensor

The average reflectance spectrum across a specified surface area is determined by the non-imaging sensor without retaining any spatial information, where variables like focal length, field of view and distance to the object define the size of the measured region. These sensors are generally portable, lightweight and do not need complex mounting platforms, making them practical for field use. These sensors have a high spectral resolution of 1–3 nm and a spectral range of 300–2500 nm.

Spectrometers like ASD FieldSpec, which are used to identify Fusarium head blight in wheat, are among the most widely used non-imaging tools (16), spectral vegetation characteristics (SVC), used in detecting potyvirus potato virus Y (PVY) in potato plants (17), ImSpector, used in detecting wheat rust (18) and STS-VIS spectrometer suitable for use on unmanned aerial vehicles (UAVs) (19). These spectrometers have been widely used in labs, greenhouses and in the field for assessing plant health and diseases. Compared to imaging sensors at similar distances, non-imaging sensors have a poorer spatial resolution since their spectral data is averaged over a certain region inside their range of view. As a result, despite the limitation of using non-imaging spectrometers in detecting diseases, they can potentially detect pre-symptomatic physiological changes if the disease-induced spectral changes are detectable within their measured field of

© The Author(s) 2026. Creative Commons CC BY 4.0. Published by Horizon e-Publishing Group.
https://doi.org/10.14719/pst.17031

view, since the output signal from the spectrometer reflects the average spectrum of healthy and diseased tissues in the sample area (14). However, these sensors are suitable for rapid evaluation of plants in fields and greenhouses (15).

Non-imaging hyperspectral signatures acquired using VIS-NIR spectrometer effectively differentiated healthy from diseased wheat leaves and ears (*Septoria tritici* blotch and *Stagonospora nodorum* blotch) by analysing spectral reflectance patterns, particularly in the red edge region where quantile spread increased systematically with disease severity (20).

Imaging sensors

Pixel-wise spectral identification is made possible by a transition from a non-imaging spectroradiometer to hyperspectral imaging, making it possible to detect subtle modifications characteristic of early-stage plant diseases. Spectral signature changes in host tissue can be identified not only at primary symptom sites and across subsequent disease stages, but also during pre-symptomatic phases and for localised tissue effects, thereby providing valuable insights into the underlying process of plant biology and fungal pathogenesis (21).

The imaging hyperspectral sensors identify the spectral bands for each pixel of the acquired image by combining spectral and spatial resolutions. The reflectance values for each spectral band that the hyperspectral sensor measured make up each pixel's own spectral signature in the image. Consequently, the final image is a hyperspectral data cube with two spatial dimensions and one spectral dimension (15).

Imaging hyperspectral sensors are preferable over non-imaging hyperspectral sensors as their spatial dimension gives additional details on gradient, colour and shape, so imaging hyperspectral sensors can be applied for site-specific and targeted field management, abiotic and biotic stress screening and thus support sustainable agriculture (16).

Depending on the sensors' configuration, a hypercube can be acquired by four different methods, namely whisk-broom, push-broom, spectral scanner and hyperspectral snapshot (13). Hyperspectral imaging sensors often only cover a narrow spectral range, like SWIR (1000–2500 nm) or VNIR (300–1000 nm). The spectral resolution of these sensors ranges from 1–7 nm. The distance between the object and the sensor determines the spatial resolution and ranges from micrometres to centimetres.

Whisk-broom and push-broom cameras represent the most frequently used point scanning and linear scanning sensors in hyperspectral imaging research. These scanning sensors require either the object or the camera to be in motion during the acquisition of images or data from scenes. Some examples of popular scanning cameras commonly employed in scientific research are Specim, Headwall, Photonfocus and Pika L and these devices are usually mounted on specific moving platforms for linear motion and stabilisation in laboratory environments. Based on the size of the measured area, these scanning sensors have a considerable image acquisition time, which makes it difficult to capture moving objects (14).

Liquid crystal tunable filter (LCTF) pass filters, which only allow specific wavelengths to pass through, are employed by spectral scanning sensors to obtain two dimensional (2D) spatial images for each wavelength without the need for a moving object or sensor in order to obtain a hypercube. Hence, acquisition is faster than other scanning methods like point and line scan, but due to the difference in timing of capturing the bands, inconsistency may arise when the object is in motion (22).

Snapshot sensors operate using a mosaic approach that is similar to RGB camera sensors but capture the entire hypercube instantly instead of using a scanning process, resulting in high recording rates but with low spatial resolution. It can be used in UAV due to their small size and shorter acquisition time. Some snapshot sensors used are Rikola Fabry-Perot interferometer (FPI)-based snapshot hyperspectral camera mounted on a UAV for potato late blight detection (23). Cubert UHD 185 FireFly snapshot hyperspectral camera mounted on a UAV for vegetation monitoring in a barley experiment (24).

Hyperspectral sensor setup

A hyperspectral sensor, an artificial or natural light source and a control device for measuring and storing hyperspectral images make up a typical hyperspectral sensor configuration. In addition to being handheld, these parts can be installed on a variety of carrier platforms, including automobiles, tractors, UAVs, robots, drones, aeroplanes and satellites. The appropriate wavelength range and object of interest are taken into consideration when choosing an imaging detector. Charge-coupled devices built of silicon and complementary metal-oxide semiconductors are the most widely used detectors for visible and near-infrared wavelengths (25). These are used in several sensing types, including full-frame cameras, push-broom cameras and whisk-broom scanners. One dimension of spectral information and two dimensions of spatial information are provided by the hyperspectral data cube that contains the data acquired through HSI (16).

In fact, the "Hypercart," a ground-based proximal sensing platform, was created to obtain high-resolution hyperspectral images of potato crops in field settings. The Hypercart setup included an aluminium framework with a motor-driven translational stage equipped with hyperspectral sensors and 18 halogen spotlights to ensure controlled and uniform illumination. Crop measurements were collected at a height of 0.60 m from the crop surface, yielding a spatial resolution of 0.30 mm per pixel. The hyperspectral imaging system was based on a push-broom system integrated with prism-grating-prism (PGP) spectroscopy system (Imspector V9, Specim) covering a wavelength range from 430–900 nm at a 7 nm spectral resolution together

© The Author(s) 2026. Creative Commons CC BY 4.0. Published by Horizon e-Publishing Group.
https://doi.org/10.14719/pst.17031

with a high-speed camera (Pike F421B). For capturing images, the Hypercart was wrapped in black cloth in order to prevent exposure to external illumination. This was done in an effort to reduce the impact of different lighting conditions on the surroundings while collecting data. With this configuration, *Alternaria solani* lesions in potato crops could be accurately detected and mapped using high-resolution hyperspectral imaging (26).

The push-broom sensors are highly spectrally accurate, but they are susceptible to any movement on the side and lighting variations. The snapshot sensors are preferred for real-time or handheld field applications but are more practical in terms of speed and robustness. The Hypercart/ground-based platforms are the most controllable and have the best resolutions but are not practical for large-scale monitoring.

Although higher spectral resolution increases biological sensitivity, it frequently comes at the expense of processing time, data volume and spatial coverage-a limitation for large-scale or real-time deployment. On the other hand, systems with coarser spectral but finer spatial resolution prioritise field usability and scalability over detection sensitivity, suggesting that there isn't a single configuration that works well in every deployment scenario.

Spectral characteristics of healthy and diseased plants

Light striking plant tissue is reflected, scattered, absorbed, or transmitted depending on the wavelength. In healthy plants, this spectral reflectance pattern is shaped by biochemical composition and its internal leaf structure (27). Photosynthetic pigments (carotenoids, anthocyanins and chlorophylls) absorb the majority of light in the visible wavelength range (400–700 nm), producing low reflectance except for the 550 nm green reflection peak in healthy plants. The leaf's cellular structure determines reflection in the NIF (700–1100 nm) range and scattering by air pockets between plant cells will result in increased reflectance. In the SWIR (1100–2500 nm), reflectance mainly depends on water content, proteins and carbonaceous materials in the plant (3).

Physiological stress from pests, pathogens, drought and nutrient deficiency disrupts the plant’s internal chemistry, altering leaf coloration, leaf size, leaf surface water evaporation and canopy architecture. These changes shift reflectance and absorption patterns, producing measurable spectral differences between normal and stressed plants (28).

Plant-pathogen interactions are characterised by distinct spatial and temporal dynamics, each influencing different portions of the electromagnetic spectrum in specific ways. Comprehending the cause-and-effect relationships between plant physiological changes and associated spectral responses offers a useful foundation for examining plant biochemistry and creating focused experimental studies (1).

Hyperspectral imaging proves to be very successful in detecting such minor spectral reflectance differences and the resulting data has enabled several ML algorithms for automated disease classification. This involves feature extraction from the spectral data, training the classification algorithm using samples of healthy and infected plants and then applying the trained model to the new data for disease prediction. One common feature extraction approach relies on calculating VIs tied to specific plant characteristics; however, most such indices are not specifically designed to distinguish between healthy and diseased states of plants (29).

Pre-processing of hyperspectral data

Enhancing contrast, removing noise, lowering data dimensionality and computational complexity and ensuring data accuracy are the primary goals of data pre-processing. Numerous elements, such as sensor noise and error, platform stability, environmental factors, light source and background conditions, affect the quality of hyperspectral data. Preprocessing is used to eliminate distortions such as curvature effects, sensor noise and other instrumental errors that may arise during data acquisition (14). Hyperspectral reflectance signals of non-imaging sensors can be easily pre-processed. The direct deletion technique is used in numerous studies to eliminate abnormal wavebands. Spectral smoothing and filtering are also used in pre-processing. Geometric correction, atmospheric calibration and spectral calibration are pre-processing techniques used in hyperspectral data imaging (1, 30).

Atmospheric correction

Atmospheric calibration is mostly used in satellite-scale data analysis due to the surface reflectivity inaccuracy caused by air scattering and absorption (1). This step is used for imaging hyperspectral data.

Geometric correction

For field, low-altitude, aerial and satellite-scale data processing, geometric correction is mostly necessary due to the geometric distortion caused by platform tilt, terrain changes, etc. (1). This step is carried out for imaging hyperspectral data. It is used to correct image distortion by transforming each spectral channel to a standard reference axis. This process aligns the image with real-world coordinates, such as map coordinates. The most common method is ground control point (GCP)-based correction. Ground control points are common points found in both the distorted image and the reference map. During correction, control points are selected and interpolation is performed to align the image correctly. Resampling methods are used along with geometric correction to assign new pixel values. Common resampling methods include:

- Nearest neighbour: determines the value of the closest pixel.

© The Author(s) 2026. Creative Commons CC BY 4.0. Published by Horizon e-Publishing Group.
https://doi.org/10.14719/pst.17031

- Bilinear interpolation – calculates pixel values using nearby pixels.
- Bicubic interpolation – uses surrounding pixels to produce smoother results.

Geometric correction improves the spatial accuracy of hyperspectral images. It helps reduce errors caused by distortion, sensor movement and scanning conditions (31).

Spectral correction

Spectral calibration is necessary for hyperspectral data, both imaging and non-imaging and is a process which involves complex algorithms (16). Methods such as radiation transfer models, spectral interpolation and spectral normalisation are employed (1). Image pre-processing typically consists of image masking, contrast enhancement and edge detection. For plant disease identification and image analysis, image enhancement may be the most important stage. Eliminating data noise and emphasising the qualities of the desired attributes are its main goals. Numerous methods, including spectral smoothing (moving average smoothing, minimum noise fraction rotation, Savitzky–Golay smoothing, etc.), data filtering (Gaussian filtering, linear filtering, etc.) and image enhancement (histogram equalisation, homomorphic filtering, etc.), can be employed to accomplish these goals (1). Other methods like Fourier transform and wavelet transform are also used to reduce noise. Baseline shifts in the spectrum are corrected using the first and second derivatives. To reduce spectral variation brought on by scattering, standard normal variate (SNV) and multiplicative scatter correction (MSC) are employed (14).

Savitzky-Golay filter or digital smoothing polynomial filter (DISPO) is a digital filter extensively used for data smoothing and differentiation purposes. It smooths digital data points by fitting segments of adjacent data points into a polynomial function of low degree using the linear least squares convolution, improving accuracy without distorting the tendency of the signal. This algorithm entails establishing a constant-sized and odd-numbered window, choosing the degree of the polynomial to be fitted, applying least squares fit locally within the window and calculating values of the polynomial at the middle of each window, thus generating the output. Savitzky-Golay filters are ideal for reducing least squares error, so efficiently conserving high-frequency signal components, in contrast to traditional finite impulse response (FIR) filters that average and eliminate high-frequency material along with noise. However, this filter provides poor noise reduction performance above the cutoff frequency and the filtering close to the data boundaries is prone to artifacts when computing derivatives (32).

Image pre-processing for the extraction of *Fusarium* head blight-infected kernels using hyperspectral microscopes, white reference and dark-current reference images were used to adjust the raw images in order to get the calibrated reflectance images. Since wheat spikelets have curved surfaces, uneven light exposure occurred in the hyperspectral images. To minimise this effect, relative spectral images were obtained by normalising each pixel with its maximum reflectance value for further analysis. In order to distinguish wheat spikelets from the background and reduce background interference during classification, threshold segmentation was also used (28). When choosing a pre-processing method, the image's type and quality are crucial (1).

Dimensionality reduction

Principal component analysis (PCA) or multivariate curve resolution (MCR) are two methods used to reduce the dimensionality of the initial image data. To do this, the unfolded three-dimensional array is divided into a set of two sub-matrices (the loading and score matrices). The primary and relevant information is kept in the score images (which include the spatial information and loadings with the spectral information), while the noisy information is eliminated in the residuals (33). Other dimensionality reduction methods used to analyse the whole spectrum include the minimum noise fraction algorithm, linear discriminant analysis, stepwise discriminant analysis and partial least square discriminant analysis (14, 31, 34).

Calibration

The hyperspectral image's spectral and spatial data are standardised through the calibration procedure. This procedure will guarantee the precision and coherence of data gathered under various circumstances. Moreover, the calibration process eliminates image curvature effects and instrumentation errors. The most popular form of calibration is reflection calibration. There are two forms of reference images used in this type of calibration: The black reference image was obtained by completely covering the camera lens with an opaque cap. A whiteboard, like Teflon, which reflects almost all light, can be used to create a white reference image. The following formula is used to adjust the raw hyperspectral image using these reference images:

$$R = \frac{I_S - I_D}{I_W - I_D}$$

where,

R = corrected hyperspectral image

I_s = raw hyperspectral image

I_D = dark image

I_W = white reference image

To remove surface curvature effects, methods such as spectral image normalisation, adaptive spherical transform and Lambert transform are used (14).

Image mosaicing

After crop image collection, multiple small-range images must be spliced into a complete large image by matching same-name pixels between the overlapping frames. Geometric reference boards were installed in

© The Author(s) 2026. Creative Commons CC BY 4.0. Published by Horizon e-Publishing Group.
https://doi.org/10.14719/pst.17031

various navigation belts as global positioning system (GPS) reference points to improve the accuracy of image mosaics. This allowed for the creation of successive mosaics based on precise geographic coordinates. The GPS-tagged images were processed through software like Agisoft PhotoScan, which is capable of stitching images automatically and Pix4Dmapper offers automated image stitching capabilities and enables production of high-precision orthographic projection images (35, 36).

In addition to classical correction methods, deep-learning-based approaches have started to complement existing pre-processing methods. The use of hyperspectral imaging and deep learning can be used to detect viral diseases at an early stage along with performing signal extraction of relevant features without using any additional pre-processing techniques. This is indicative of the shift from classical statistical correction techniques to learned, task-adaptive pre-processing methods (37).

Feature extraction techniques

The feature extraction process is considered the most crucial phase in hyperspectral-based classification, particularly for detecting plant diseases. The goal of feature extraction is the formation of new feature vectors using the optimisation of the spectral, spatial and texture information. Subsequently, the developed feature vectors are then fed into various classifiers or ML algorithms to increase the precision and resilience of disease identification (14).

Feature extraction techniques employ specific linear transformations to effectively diminish noise present in feature datasets. These algorithms are typically organised into two categories: supervised and unsupervised methods. Unsupervised methods encompass PCA, maximum noise fraction (MNF) and independent component analysis (ICA), whereas linear discriminant analysis (LDA) represents a supervised approach. Despite their different architectures, both methodologies serve a common purpose: they convert hyperspectral imagery from high-dimensional space into a more compact, lower-dimensional representation while preserving the essential information content within a reduced set of principal components (38).

High-dimensional data is reduced to a smaller collection of uncorrelated variables known as principal components using a dimensionality reduction method called PCA. The Hughes phenomenon and the curse of dimensionality, which together cause classification accuracy to drastically decline when the number of spectral features greatly exceeds the available training samples, are two major obstacles that PCA helps to overcome in hyperspectral classification. Principal component analysis is utilised in hyperspectral imaging to handle the enormous complexity of spectral data in order to detect powdery mildew in wine grapes (39).

Independent components discriminant analysis (ICDA) can be described as a non-parametric discriminant analysis that employs the ICA technique as the main approach for extracting independent features out of hyperspectral high-dimensional data. As a result, it becomes possible to overcome the curse of dimensionality that negatively affects Bayesian classifier performance. After applying the transformation that maps data onto the independent feature space using ICA, the class-conditional multivariate density estimation problem that becomes difficult to tackle in high dimensionality turns into a much simpler product of univariate estimations for each of the extracted independent components. The density function of each extracted independent feature is estimated using a non-parametric kernel density estimator and the Bayes formula makes use of those estimations (40).

The MNF is a dimensionality reduction technique utilised in hyperspectral images that transforms data from high-dimensional spectra into lower-dimensional space by reordering principal components based on signal-to-noise ratio (SNR), while PCA orders them according to image information. The MNF algorithm is a very effective method in terms of dealing with the problem of noise in images and works by applying a linear transformation on the high-dimensional data to produce low-dimensional data, whereby noise covariance matrices are determined through a multiple linear regression of the residuals between image blocks. This approach not only lowers the cost of computation significantly but also brings down the execution time to roughly one fifth of the baseline while improving classification accuracy and robustness against noise (41).

The supervised dimensionality reduction technique known as linear discriminant analysis (LDA) is used to extract spectral information for classification by reducing the number of spectral bands in a hyperspectral image. The technique transforms the high-dimensional spectral feature space into a low-dimensional spectral feature space using the image's known class labels. As a result, class separation is improved to address overfitting problems by lowering parameter estimate error and speeding up classification computation. Nevertheless, the information needed for classification is retained in a very small number of linear discriminant components despite the decreased spectral bands (42). The LDA was applied to the spectral reflectance analysis of olive trees (*Olea europaea* L.) to extract the most important features that discriminate between normal trees and trees affected by *Fomitiporia mediterranea*. Through LDA, the high-dimensional spectral information was transformed into linear combinations having maximum separation between classes while minimising variance within each class. The extracted linear discriminants served as the key features enabling classification and also achieving strong discrimination accuracy (43).

Partial least squares (PLS) were used as a dimensionality reduction and feature extraction method to address the problem of high-dimensional hyperspectral data obtained from infested potato tubers

© The Author(s) 2026. Creative Commons CC BY 4.0. Published by Horizon e-Publishing Group.
https://doi.org/10.14719/pst.17031

with root-knot nematodes (*Meloidogyne* spp.). Partial least squares reduced the hyperspectral space to a lower dimension by extracting latent variables having maximum covariance between the spectral reflectance data and the target variable, i.e., infestation. Thus, redundant hyperspectral information is compressed into useful components through PLS transformation, in which these extracted PLS components can be used as input features to the classification models for effective discrimination of healthy and diseased potatoes (44).

Image segmentation is carried out to separate the target items from the background prior to formal spectral analysis or to generate the areas of interest (ROIs) required for further data extraction and make a mask (35). The different segmentation techniques include the watershed algorithm, K-means, threshold-based and edge detection (14).

Segmentation is the process of splitting an image into several segments, each representing a homogeneous area having similar spectral characteristics. It serves as the initial step in image preprocessing after calibrating the image in the hyperspectral image analysis process. It aids in background elimination, makes the data simpler and improves the efficiency of future classification activities, as well as helping in reducing the size of data. Many different methods are used for automatic image segmentation in hyperspectral imaging, such as clustering, morphology operations, edge detection, PCA and vegetative index such as normalised difference vegetation index (NDVI), along with deep neural network models developed using RGB images producing binary masks of the hyperspectral cube. The selection of segmentation depends upon the purpose and the type of dataset. It is crucial for reflectance studies in that it ensures purity of the spectral information in the region of interest by getting rid of the signals outside that region (12).

Vegetation indices-based segmentation

Vegetation indices are commonly used to extract spectral features by combining two or more wavelengths. Analysis of infected leaves indicates a change in the amount of green colour of the infected part compared to normal plants and VIs, which are metrics of greenness in remote sensing image analysis, are determined using the captured images of the infected parts and are employed to remove the infected parts from the images. The computed values of VIs are used to segment the images and hence extract the infected parts from the images of the leaves based on the measurable drop in greenness caused by disease. This VI-based segmentation approach provides a robust and automated means of isolating lesion areas on rice leaves, which then feeds into the classification stage to distinguish between brown spot and blast diseases (45).

Full spectrum feature extraction uses reflectance values from all wavelengths. This preserves complete spectral information as mean reflectance for each wavelength for all pixels in a plant leaf was used as features. This method allows ML models to identify complex spectral patterns and provides better classification accuracy than using selected indices alone (29).

Probabilistic topic modelling is a data-driven feature extraction method. It is an unsupervised ML method used to reduce hyperspectral data dimensions and extract useful features for disease classification (46). The latent dirichlet allocation (LDA) model is trained to identify hidden spectral patterns (topics) within large datasets. Each hyperspectral pixel is treated as a document and each wavelength-reflectance pair is treated as a word. The algorithm analyses these spectral “documents” and discovers hidden spectral patterns called topics. Each topic represents a characteristic spectral signature and each pixel is assigned a probability distribution over multiple topics. The LDA works through a generative process: first, a topic is selected based on probability and then a spectral word is chosen from that topic. By repeating this process, LDA learns the relationship between spectral features and their topic distributions (29).

In plant disease detection, LDA helps to minimise the high dimensionality of hyperspectral data by transforming complex spectral information into a smaller set of meaningful topic proportions. These topic proportions capture subtle spectral differences between healthy and diseased tissues, making them highly useful for classification and disease monitoring (47).

Enabling deep architectures to automatically learn hierarchical and discriminative spectral-spatial patterns rather than depending on manually created indices, integrating deep learning with conventional ML enhances feature representation for plant disease diagnosis. This hybrid approach, which reflects a larger trend in the field toward automated, learned feature extraction over manually created spectral indices and statistical techniques, combines the interpretability and efficiency of traditional classifiers with the representational strength of deep learning (48). In deep learning-based feature extraction for hyperspectral disease detection, interpretability remains a largely unresolved challenge. One of the few attempts to address the "black box" limitation applies explainable 3D deep learning to hyperspectral images, using saliency-based visualisation to reveal which spectral-spatial regions drive the model's classification decisions (49, 50). The lack of comparable work highlights explainability as an underdeveloped area relative to the rapid growth of deep learning-based feature extraction methods in this field.

Vegetation indices for disease detection

Hyperspectral reflectance measurements are usually transformed into VIs to provide more relevant information or adjust for atmospheric or soil-related background interference. Vegetation indices are arithmetical combinations of reflectance in various spectral wavebands which correspond to particular plant biophysical characteristics like the amount of chlorophyll, biomass, water content, etc. Vegetation indices were calculated by combining two or more

© The Author(s) 2026. Creative Commons CC BY 4.0. Published by Horizon e-Publishing Group.
https://doi.org/10.14719/pst.17031

spectral wavelengths to extract features from spectral reflectance that highlight the biophysical and spectral characteristics of green vegetation. It aids in distinguishing them from other aspects of the image. A few VIs employ a variety of wavelength measurements to explain physiological characteristics of plants and other vegetation generic characteristics or the growth parameters of a particular plant (51).

The mechanism through which vegetative indices operate is by assessing the contrast between the red and near-infrared reflectance of the vegetation. This works well since the red spectrum is absorbed by the chlorophyll while the leaf mesophyll structures cause the NIR reflectance. In the event where there is a huge difference between the red and NIR reflectance, it means that there are plenty of healthy plants. On the other hand, when there is very little contrast between the red and NIR reflectance, it can be concluded that there is less vegetation within the area (51).

The use of a single VI for plant disease detection often lacks sufficient discriminatory power to distinguish diseased from healthy plants and also different vegetation indices correspond to different plant properties (29). A more effective approach involves combining multiple vegetation indices to capture diverse spectral characteristics that respond differently to disease-induced changes in plant physiology. By integrating several indices as classification features and applying them in ML algorithms, higher accuracy and early disease detection are achieved. This multi-index approach takes into account that different diseases change plant spectral signatures differently, so disease-specific index combinations are more effective than any single index alone. The usage of multiple VIs with support vector machines to classify spectral data of sugar beetroot plants got classification accuracies of around 95 % for *Cercospora beticola* and *Uromyces betae* and more than 92 % for *Erysiphe betae* while comparing with single VI accuracy (52). Different VIs were important for different diseases, highlighting the importance of selection of disease-specific indices in developing detection systems.

Standard vegetation indices, such as NDVI, spot general plant stress but cannot tell specific diseases apart. This leaves farmers clueless about which pathogen is hitting their crops. The spectral disease indices come in to help here by using custom spectral formulas. These formulas target the unique light reflectance from each individual disease as different pathogens affect plants differently. The disease specific spectral indices are customised mathematical formulas tailored to detect particular plant pathogens (e.g., powdery mildew, rust, blight). Instead of using general VIs, developing unique spectral signatures caused by each disease's physiological effects on plants and create targeted indices that maximise sensitivity to those specific changes. This approach enables differentiation between different diseases and healthy plants using remote sensing data, allowing precise, pathogen-level diagnosis at field scale- critical for targeted disease management without unnecessary fungicide application (53). Table 1. summarises spectral vegetation indices commonly applied in disease detection.

Machine learning approaches in data analysis

After the required preprocessing is completed and the data has been separated into training and test sets, the final stage in image analysis is to choose a model and apply it to the data. The model is trained using the training dataset. Training is the most important stage in machine learning. The prepared data is fed into the ML model during training, allowing it to recognise patterns and generate predictions. The model completes the task and learns from the data (49).

Table 1. Common spectral vegetation indices used in hyperspectral plant disease detection

Sl. No	Vegetation indices	Formula	Significance	Reference
1.	Normalised difference vegetation index (NDVI)	$NDVI = \frac{(NIR - RED)}{(NIR + RED)}$	Changes in chlorophyll content, examine green and healthy vegetation	(54)
2.	Photochemical reflectance index (PRI)	$PRI = \frac{(\rho531 - \rho570)}{(\rho531 + \rho570)}$	Sensitive to carotenoid pigment changes, changes in photosynthetic effiency	(55, 56)
3.	Anthocynanin reflectance index (ARI)	$ARI = \frac{1}{\rho550} - \frac{1}{\rho700}$	Elevated anthocyanin concentration indicates deteriorating vegetation, allowing anthocyanin- based spectral indices to serve as diagnostic markers of vegetation stress	(57)
4.	Modified chlorophyll absorption ratio index (MCARI)	$MCARI = \frac{(\rho701 - \rho671) - 0.2(\rho701 - \rho549)}{(\rho701 - \rho761)}$	Leaf area Index and chlorophyll estimation	(57, 58)
5.	Carotenoid reflectance index (CRI)	$CRI = \frac{1}{\rho510} - \frac{1}{\rho550}$	Vegetation under stress accumulates higher carotenoid levels, making carotenoid indices useful indicators of plant stress	(59)

© The Author(s) 2026. Creative Commons CC BY 4.0. Published by Horizon e-Publishing Group.
https://doi.org/10.14719/pst.17031

6.	Structure insensitive pigment index (SIPI)	$SIPI = \frac{(\rho800 - \rho445)}{(\rho800 + \rho680)}$	Increases the index's sensitivity to the bulk carotenoids to chlorophyll ratio	(56)
7.	Normalized difference nitrogen index (NDNI)	$NDNI = \frac{\log\left(\frac{1}{\rho1510}\right) - \log\left(\frac{1}{\rho1680}\right)}{\log\left(\frac{1}{\rho1510}\right) + \log\left(\frac{1}{\rho1680}\right)}$	Measures relative nitrogen content in plant canopies	(48)
8.	Plant pigment ratio (PPR)	$PPR = \frac{(\rho550 - \rho450)}{(\rho550 + \rho450)}$	Detects foliar pigments by the ratio of green to blue reflectance. A high value is obtained for strongly pigmented vegetation and a low value for weakly pigmented foliage.	(60, 61)
9.	Plant senescence reflectance index (PSRI)	$PSRI = \frac{(\rho660 - \rho510)}{(\rho760}$	Detect the carotenoid to chlorophyll ratio to quantitatively measure leaf senescence and fruit ripening	(61)
10.	Green normalised difference vegetation index (GNDVI)	$GNDVI = \frac{(\rho750 - \rho540 + \rho570)}{(\rho750 + \rho540 - \rho570)}$	Similar to NDVI but measures the green spectrum, Sensitive to chlorophyll concentration	(51, 61)
11.	Red green index	$RGI = \frac{\rho690}{\rho550}$	Indicator of plant chlorophyll content and physiological condition	(61)
12.	Triangular vegetation index (TVI)	$TVI = 0.5 * (120(\rho750 - \rho550) - 200(\rho670 - \rho550))$	The area of a hypothetical triangle with vertices at red, green and NIR wavelengths is the basis for TVI. It is affected by both the leaf area index and the amount of chlorophyll. When the absorption of chlorophyll is high, the triangle's total area increases.	(51)
13.	Modified simple ratio (MSR)	$MSR = \frac{\frac{NIR}{Red} - 1}{\sqrt{\frac{NIR}{Red}} + 1}$	Enhances the sensitivity of vegetation biophysical measurements	(57, 62)
14.	Transformed chlorophyll absorption index (TCARI)	$TCARI = 3\{(\rho700 - 670\ 0.2 * (\rho700 - 550) * \frac{\rho700}{\rho670}\}$	Measures chlorophyll content and leaf area index with minimal soil effects	(57, 58, 61)
15.	Nitrogen reflectance index (NRI)	$NRI = \frac{(\rho570 - \rho670)}{(\rho570 + \rho670)}$	Assess plant nitrogen status	(61, 63)
16.	Red edge normalised difference vegetation index (RENDVI)	$RENDVI = \frac{(\rho750 - \rho705)}{(\rho750 + \rho705)}$	Modifying the NDVI by using red edge instead of absorption and reflectance peaks to improve sensitivity of small changes in canopy foliage content, gap fraction and senescence	(61)
17.	Simple ratio (SR)	$SR = \frac{\rho900}{\rho680}$	Estimate vegetation biophysical parameters like leaf area index and photosynthetically active radiation absorption	(29, 51, 62)
18.	Normalised difference lignin index (NDLI)	$NDLI = \frac{\log\frac{1}{\rho1754} - \log\frac{1}{\rho1680}}{\log\frac{1}{\rho1754} + \log\frac{1}{\rho1680}}$	Estimate lignin content in vegetation based on reflectance at specific infrared wavelengths	(29, 48, 51)

© The Author(s) 2026. Creative Commons CC BY 4.0. Published by Horizon e-Publishing Group.
https://doi.org/10.14719/pst.17031

19.	Red- edge stress vegetation index (RVSI)	$RSVI = \frac{(\rho712 + \rho752)}{2} - \rho732$	Detect plant stress by analysing reflectance in the red edge wavelength region	(57, 64)
20.	Normalised pigment chlorophyll ratio index (NPCI)	$NCPI = \frac{(\rho680 - \rho430)}{(\rho680 + \rho430)}$	Measure carotenoid-to-chlorophyll ratio for assess nitrogen status and senescence	(56, 57, 63)
21.	Greenness index (GI)	$GI = \frac{\rho554}{\rho677}$	Assess vegetation greenness and detecting changes in leaf pigmentation	(51, 65)
22.	Water band index (WBI)	$WBI = \frac{\rho900}{\rho970}$	Evaluate water content and stress in vegetation	(56, 65)
23.	Chlorophyll index (CI)	$CI = \frac{\rho840}{\rho570} - 1$	Estimate chlorophyll concentration	(66)
24.	Ratio analysis of reflectance of spectral chlorophyll a (RARSa)	$RARSa = \frac{\rho675}{\rho700}$	Estimate chlorophyll a concentration	(61, 66, 67)
25.	Ratio analysis of reflectance of spectral chlorophyll b (RARSb)	$RARSb = \frac{\rho675}{(\rho700 * \rho650)}$	Estimate chlorophyll b concentration	(61, 66, 67)
26.	Ratio analysis of reflectance of spectral chlorophyll c (RARSc)	$RARSc = \frac{\rho760}{\rho500}$	Estimate carotenoids concentration	(61, 66, 67)
27.	Pigment specific simple ratio (PSSRa)	$PSSRa = \frac{\rho800}{\rho680}$	Estimate chlorophyll a concentration, strong linear relationships with pigment concentration	(29, 68)
28.	Pigment specific simple ratio (PSSRb)	$PSSRb = \frac{\rho800}{\rho635}$	Estimate chlorophyll b concentration, strong linear relationships with pigment concentration	(29, 68)
29.	Canopy chlorophyll index (CCI)	$CCI = \frac{(NIR - RED\ EDGE)}{(NIR + RED\ EDGE)} \Big/ \frac{(NIR - RED)}{(NIR + RED)}$	2D remote sensing index calculated from NDVI and NDRE to analyse the chlorophyll content in vegetation isolating leaf signal from soil background	(51)
30.	Modified triangular vegetation index (MTVI)	$MTVI = 1.2 * (1.2(\rho800 - \rho550) - 2.5 * (\rho670 - \rho550))$	Measure leaf area index, less sensitive to chlorophyll content variations	(58, 61, 66)
31.	Health index (HI)	$HI = \frac{(\rho739 - \rho402)}{(\rho739 + \rho402)} + 0.5 * \rho403$	Detect and classify whether plant leaves are healthy or diseased based on their reflectance charateristics	(56, 64)
	Disease specific indices			
32.	Yellow rust index (YRI)	$YRI = \frac{(\rho730 - \rho419)}{(\rho730 + \rho419)} + 0.5 * \rho403$	Detect yellow rust	(56, 64)
33.	Powdery mildew-index (PMI)	$PMI = \frac{(\rho515 - \rho698)}{(\rho515 + \rho698)} + 0.5 * \rho738$	Identify powdery mildew infected leaves	(56, 64)

ρ – reflectance in nm; NIR: near infra-red band; red: red band; red edge: red edge band.

Machine learning methods are able to handle hundreds of spectral bands and have become well established tools for detecting, quantifying and characterising plant diseases in field, greenhouse and laboratory conditions. These methods infer or learn model properties from the data itself rather than employing a predetermined model. Supervised methods require labelled training datasets. While unsupervised methods operate without the training datasets (16).

Supervised machine learning

Supervised ML models employ labelled datasets with sensor data, images, or additional pertinent information to identify patterns associated with different crops or

© The Author(s) 2026. Creative Commons CC BY 4.0. Published by Horizon e-Publishing Group.
https://doi.org/10.14719/pst.17031

diseases (6). The models can be either regression models (for predicting and analysing the association between the target variables and the spectral response) or classification models (for detecting and classifying diseases), depending on the study's goals (14). Table 2. summarises classification and detection accuracies reported across the reviewed studies, along with the scale, sensor platform, feature set and model where available, to enable direct comparison across crop–pathogen systems.

Classification models

Classification models classify each data sample based on their classes by training on labelled data. These models can operate at two levels: 1) the image level, where the overall content of an image (or an entire plant when only one is present) is interpreted and assigned a category; 2) pixel level, in which each pixel in the image is given a meaningful description, such as "healthy tissue" or "disease symptom," resulting in a fully classified image (15).

The commonly used method for classifying pixels is the spectral angle mapper (SAM) that uses a cosine distance measure in assessing similarity among spectra. It involves assigning the class for all pixels that lie within a certain angle range in the feature region compared to the reference data point. The major advantage of using cosine distance is that it takes care of the scaling effects arising from differences in lighting conditions among other issues, hence making comparisons among the spectra easy. The SAM was applied in detecting and locating different disease symptoms on sugar beets caused by three diseases (21), detecting citrus canker in citrus plants (50) and fusarium head blight in wheat ears (69).

Table 2. Cross-study comparison of hyperspectral disease detection methods and their reported performance metrics

Crop	Pathogen	Country	Leaf/ canopy/ field	Sensor and platform	Spectral range	Feature set	Model	N (train/test)	Reported metric value
Sugar beet	Cercospora leaf spot (*Cercospora beticola*)	Germany	Leaf	ImSpector V10E line-scan hyperspectral imaging spectrograph + mirror scanner, controlled chamber, ASD-Pro-Lamps illumination	400–1000 nm (2.8 nm spectral resolution)	. Pixel-wise reflectance spectra; . 3 endmember classes: healthy / margin / necrotic centre	Spectral angle mapper (SAM)	. 20 fully developed symptoms/ disease for spectral signature extraction; . 10 symptomatic areas analyzed daily; pixel-level classification	8 dai: 98.90 % accuracy, κ = 0.99, 0 % diseased area classified 11 dai: 89.01 % accuracy, κ = 0.53, 6.56 % diseased 14 dai: 96.58 % accuracy, κ = 0.92, 7.61 % diseased 17 dai: 98.73 % accuracy, κ = 0.98, 20.92 % diseased
Citrus	Huanglongbing (HLB) / citrus greening	USA	Canopy (pixel/tree-canopy level)	. AISA EAGLE VNIR hyperspectral imager, airborne (640 m altitude); . WorldView-2 satellite multispectral (for comparison)	. 400–1000 nm, 128 bands, 5 nm resolution (HS); . WV-2: 8 bands, 400–1040 nm (MS)	. Savitzky–Golay-smoothed reflectance spectra; . SVM-derived canopy mask; . VCA pure endmembers; spectral angle (SAM); . red-edge position (REP, linear extrapolation)	. ESAM (SVM mask → VCA endmember extraction → SAM classification → REP false-positive filtering); . compared against Mahalanobis distance and K-means	. Block 8a (mature): 26 healthy + 23 HLB / 25 healthy + 22 HLB; . Block 2b (intermediate): 14/14 HLB; Block 5c (young): 33/33 HLB	Detection accuracy - . Block 8a: 82.6 % (calibration), 86.3 % (validation); . Block 2b: 64.2 %/71.4 %; . Block 5c: 72.7 %/63.6 %. MS image (SAM): 78.2 %/63.6 %
Wheat	Fusarium head blight	Germany	Ear (organ-level, both lab and field)	. Lab hyperspectral pushbroom imager (ImSpector V10E + Pixelfly qe CCD),	· 400–1000 nm, 2.5 nm resolution (HS); · fluorescence at 685–700 nm emission band (CFA)	. Raw reflectance spectra (512 bands) for SAM; pixelwise Fv/Fm distributions and cumulative Fv/Fm curve for	. Spectral Angle Mapper (SAM, ROI-based endmembers) for HS; cumulative	. HS: 12 infected + 12 control ears (time series); CFA lab: 6 infected + 6 control	. HS-SAM vs. visual rating: R^2=0.964; best detection window 14 ± 2 dai, up to 50 % severity; CFA lab:

© The Author(s) 2026. Creative Commons CC BY 4.0. Published by Horizon e-Publishing Group.
https://doi.org/10.14719/pst.17031

				bench-mounted; FluorCAM 700MF chlorophyll fluorescence imager, bench and field (shielded box)		CFA	Fv/Fm threshold (0.3) classification for CFA	(time series), 15 ears at BBCH75; · CFA field: 30 ears (of 50 imaged)	differentiates in 10 % severity steps from 6 dai; · CFA field: R^2 = 0.658 (RMSE=17 %), rising to R^2 = 0.80 after outlier removal
Tomato	Bacterial leaf spot (*Xanthomonas* spp.)	USA	Leaf	Resonon benchtop HSI (Pika L + Pika NIR320), lab imaging	400–1700 nm (VISNIR 388–1025 nm + SWIR 896–1715 nm)	Full spectra (leaf- and pixel-level) and 14 vegetation indices (VIs)	LDA, SVM, KNN, RF, GBM, XGBoost, MLP (best: LDA for full spectra; RF for pixel/VI data)	Leaf-level: 36–92 leaves/stage across 4 stages; pixel-level: 648 pixels/range across 9 classes	Leaf-level LDA accuracy 0.55–0.74 (VISNIR/SWIR, pre- to post-symptomatic); pixel-level RF accuracy 0.63 ± 0.13 (VISNIR), 0.57 ± 0.16 (SWIR); VI-based models outperformed raw data by 26–37 %
Sugar beet	*Cercospora beticola*, *Uromyces betae*, *Erysiphe betae*	Germany	Leaf	ASD FieldSpec Pro FR, handheld leaf-clip	400–1050 nm	8 VIs + SPAD	SVM (RBF); compared vs. DT, ANN	3,570 leaf spectra (pooled, 10-fold)	· Acc. 97 % (healthy vs. diseased); 86 % (4-class); · 65–90 % presymptomatic
Brinjal, Cluster beans, Long Beans		India	Leaf	ASD FieldSpecPro spectroradiometer, ground-based/in-lab (fibre optic, 8° FOV, halogen lamp illumination)	350–2500 nm (2151 bands), analyzed in 5 sub-regions: Visible (350–670 nm), Red Edge (671–780 nm), NIR (781–1000 nm), SWI (1301–1500 nm), SWII (1701–1900 nm)	350–2500 nm (2151 bands), analyzed in 5 sub-regions: Visible (350–670 nm), Red Edge (671–780 nm), NIR (781–1000 nm), SWI (1301–1500 nm), SWII (1701–1900 nm)	Random Forest classifier (with PCA or LDA as pre-filter)	25 leaf samples each of Brinjal, Cluster Beans, Long Beans (healthy + infected), 10 spectral iterations/sample	Best region = Visible/Red Edge; mean accuracy (PCA): Brinjal 0.864, Cluster Beans 0.92, Long Beans 0.90 (Kappa 0.66/0.83/0.78); Long beans red edge PCA hit 1.0 accuracy/Kappa
Chardonnay wine grape (*Vitis vinifera*)	Powdery mildew (*Erysiphe necator*)	Australia	Berry (detached) and bunch (intact), lab-controlled	HySpex VNIR 1600 + HySpex SWIR-320m-e line-scan cameras, benchtop/translation stage	VNIR 400–1000 nm (3.7 nm resolution, 160 bands); SWIR 970–2500 nm (6 nm resolution, 256 bands)	LDA/PCA-reduced spectral bands + spatial-spectral texture features (mean, SD, homogeneity via integral images at multiple block sizes)	Modified Random Forest classifier (pixel-wise spectral vs. spatial-spectral texture-based)	Detached berries: 128 healthy + 136 diseased (training/CV); intact bunches: 30 (10 healthy, 10 infected, 10 severely diseased) × 2 scans = 60 images (validation)	Detached berries: accuracy up to 0.998 ± 0.003 (LDA+spatial-spectral, VNIR); intact bunches: overall accuracy improved from 0.76 (spectral-only) to 0.86 (spatial-spectral); severely diseased bunches detected with high accuracy, healthy/infected discrimination harder

© The Author(s) 2026. Creative Commons CC BY 4.0. Published by Horizon e-Publishing Group.
https://doi.org/10.14719/pst.17031

Avacado	Laurel wilt (Raffaelea lauricola)	USA	Leaf	SVC HR-1024, handheld; greenhouse + field	350–1000 nm (66 bands, 10 nm)	PCA scores (99.9 % variance)	LDA, QDA, NB, BDT	Random 75:25 split	· 249/83 (healthy vs asymptomatic); 209/69 (healthy vs symptomatic)
Cucumber	Angular leaf spot *Pseudomonas syringae* pv. *lachrymans*	China	Leaf	Line-scan HSI camera, benchtop	380–1030 nm (476 used for modeling)	Regressionco efficient-selected important wavelengths (IWs): 9 bands for Chl (408, 484, 533, 582, 686, 708, 750, 911, 976 nm); 5 bands for Car (484, 558, 675, 705, 765 nm)	PLSR (RC-PLSR)	130 calibration / 64 prediction (194 total leaves)	· Chl-HSI: Rc=0.901, Rcv=0.889, Rp=0.871, RMSEP=0.25 mg/g; · Car-HSI: Rc=0.803, Rcv=0.793, Rp=0.876, RMSEP=0.05 mg/g
Wheat	Septoria tritici blotch (*Zymoseptoria tritici*) + Stagonospora nodorum blotch (*Parastagonospora nodorum*)	Russia	Leaf and ear (in situ, field, non-imaging point measurements)	Ocean Insight "Flame" VIS-NIR non-imaging hyperspectrometer, handheld/field (0.3 nm resolution)	338–1018 nm (downsampled to 350–950 nm, smoothed to 6 nm step for NN)	Full hyperspectral reflectance signatures (100 values/curve after smoothing); red-edge slope "angle" metric derived from curve shape	Perceptron neural network (PNN), 2 layers (5+2 neurons)	2000 spectral curves/leaf dataset, 2000–4000/ear dataset; 8 leaf + 8 ear datasets total (healthy, light, medium, severe, dead)	· PNN (10,000 epochs): 0.99 accuracy, 0.94 precision, 0.89 recall, 0.91 F-score; · healthy/severe leaf classification 88.1–97.7 %; light/medium severity harder (38–66 %); · Cohen's kappa 0.90–0.98 (healthy/severe) vs. 0.13–0.64 (light/medium), overall κ=0.69
Apple	Marssonina blotch	USA	Leaf-level (indoor detached-leaf imaging), with a supplementary test on an outdoor canopy/tree image	SPECIM PS-V10E pushbroom camera, lab setup	356–1000 nm (437 bands used; 10 selected)	OSP-selected bands (mostly NIR 680–957 nm	Decision tree, weighted KNN, ensemble bagged	10,000 px (2,000 × 5 classes); 5-fold CV, no explicit train/test split; outdoor image as external test	Accuracy: 84.3 % (ensemble), 79.8 % (DT), 71.3 % (KNN)
Barley	Powdery mildew (*Blumeria graminis*)	Germany	Leaf/ cellular (microscopic)	Hyperspectral line-scan camera (Specim PFD V10E) on stereo microscope foreoptic, 7.3x magnification	400–1000 nm (analyzed 420–830 nm), 2.73 nm resolution	Full-spectrum reflectance signatures; SiVM-derived extreme components/simplex representation	Simplex Volume Maximization (data-driven matrix factorization) + Dirichlet-aggregation regression (leaf traces); LLR-based binary disease maps	3 inoculated + 4 healthy leaves per genotype (n=3 genotypes: WT, Mla12, mlo3)	Automated vs. manual spectral difference: WT −0.04 to 0.04; Mla12 −0.02 to 0.03; RSD 0.6–14.7 % across genotypes/time

© The Author(s) 2026. Creative Commons CC BY 4.0. Published by Horizon e-Publishing Group.
https://doi.org/10.14719/pst.17031

Ash	Ash dieback (*Hymenoscyphus fraxineus*)	UK	Canopy/ landscape (forest site, airborne)	Hyspex VNIR 1800 hyperspectral camera, human-crewed aircraf	· 410–1001 nm, 186 bands, 3.26 nm resolution; · 0.32 m native / 1.28 m downsampled spatial resolution	Raw pixel spectra; pixel purity η(x) via HySime + VCA unmixing; density-purity harmonic mean ζ(x); diffusion distances	PLSDA (species mapping) → Random Forest (supervised disease classes: healthy/ infected/ severely infected) vs. D-VIS (unsupervised diffusion + VCA clustering, K=2: healthy/die back)	PLSDA: 166 Madingley crowns + 256 crowns from 3 other sites; RF test set: 16 trees/class; D-VIS: n=72,775 ash pixels (401×279 scene	PLSDA accuracy 85.3 %; RF accuracy 77.1 %; D-VIS vs. RF overall accuracy 71.0 %, average accuracy 71.3 %
Tobacco	Tobacco mosaic virus (TMV)	China	Leaf	(ImSpector V10E + Hamamatsu C8484-05 CCD), benchtop	380–1023 nm (450–1000 nm/434 bands used)	SPA-selected 8 EWs; GLCM texture (contrast, correlation, entropy, homogeneity); EW+texture fusion	· PLS-DA, RF, SVM, LS-SVM, ELM, BPNN	120 samples for calibration (training) and 60 for prediction (testing)	Best: SPA-ELM overall accuracy 98.33 % (EWs); BPNN 93.33 % (texture); BPNN 95.00 % (fusion
Wheat	*Puccinia triticina* (leaf rust)	Iran	Leaf	ASD spectroradiometer (contact probe) + RGB camera (Canon IXUS 85 IS)	450–1000 nm	22 SVIs (NDVI, NBNDVI, GI, PRI, ARI, TCARI, MSR, PSRI, PhRI, TVI, RVSI, NRI, SIPI, NPCI, CARI, MCARI + derivative-based variables)	Threshold/ statistical classification (healthy vs. rust) across 10 disease-severity classes	300 spectral samples	Best: NBNDVI 83 %, NDVI 81 %, GI 77 %, ARI 75 % classification accuracy
Oilseed rape	Alternaria spp	Poland	Leaf	VNIR camera (ImSpector V10E) + SWIR camera (N25E 2/3", SPECIM) on conveyor belt; FLIR SC620 thermal camera (8–13 µm)	· 400–1000 nm (VNIR) + 1000–2500 nm (SWIR); · classification used 430–2376 nm at ~32 nm increments (61 channels)	Second-derivative transformed reflectance spectra (Savitzky-Golay, 4th-order, 11 points); raw/averaged reflectance also examined	· 8 classifiers compared (NB, SL, SVM, LibLINEAR, BNN, FT, RF, J48); · best = Back-Propagation Neural Network (BNN)	251 instances (training/testing) + 28 instances (validation)	Days-after-inoculation classification: BNN 90.5 % (train/test), 93.3 % (validation); *Alternaria* species classification: BNN 80.5 % (train/test), 82.3 % (validation)
Onion	*Burkholderia cepacia* (sour skin)	USA	Bulb/organ level (neck & shoulder region)	SWIR pushbroom hyperspectral imager: LCTF + InGaAs camera, lab chamber with halogen lamps	950–1650 nm (2 optimal bands selected: 1070 & 1400 nm)	Log-ratio image (1070/1400 nm) → 12 statistical/textural features (GLCM-based), reduced via stepwise discriminant analysis to 3	LDA on segmented pixel count (threshold= 0.45); SVM (RBF kernel, γ=1.5) on 3 image features	140 images total (75 onions × 2 timepoints, 70 inoculated + 5 controls)	Accuracy: LDA 80 % (healthy 97.14 %, diseased 62.86 %); SVM 87.14 % (healthy 81.43 %, diseased 92.86 %)

© The Author(s) 2026. Creative Commons CC BY 4.0. Published by Horizon e-Publishing Group.
https://doi.org/10.14719/pst.17031

						(max, contrast, homogeneity); also pixel-count from thresholded log-ratio images			
Soybean	Charcoal rot (*Macrophomina phaseolina*)	USA	Stem (excised, benchtop imaging)	Pika XC hyperspectral line imaging scanner (Resonon), 240 wavebands, 2.5 nm resolution	400–1000 nm	Raw hyperspectral data cubes (3D spatial-spectral patches, 64×64×240 pixels); no hand-crafted indices	3D deep convolutional neural network (3D-CNN, 2 conv+pooling layers, 2 fully-connected layers, softmax output) with class-balanced weighted binary cross-entropy loss	Training: 1090 patches (940 healthy/150 infected); Validation: 194; Test: 539 (from 111 original hyperspectral stem images: 64 healthy/47 infected)	Test accuracy 95.73 %; recall 0.92; precision 0.82; F1 (infected class) 0.87; 5-fold CV mean accuracy 95.49 % (SD 2.01 %)
Sweet/ bell pepper	Tomato spotted wilt virus (TSWV)	USA	Pixel-level within whole-plant (top-canopy) images	Hyperspectral reflectance imaging system, Specim ImSpector V10E camera mounted on a Motorman SL robotic manipulator; · lab setup with two halogen lamps at 45°	395–1005 nm (83 bands used out of full range; 8 bands sufficient after MVPCA band selection)	Pixel-wise raw reflectance spectra (83 bands), no dimensionality reduction beyond band selection; also evaluated with MVPCA/FDPC/SUBS-selected bands + OR-AC-GAN-augmented synthetic spectra	OR-AC-GAN (outlier-removal auxiliary classifier GAN); benchmarked against 1D-CNN and standard AC-GAN; final classification via built-in discriminator (or KNN when band-selected)	Training pixels: 103,769 background, 105,561 healthy, 2,071 TSWV (from 6 images); Test: 54 plants/images	Pixel accuracy 98.03 %; TSWV false-positive rate in healthy plants 1.47 % (avg, worst 8.21 %); plant-level sensitivity 92.59 %; overall plant-level classification accuracy 96.25 %

ASD: analytical Spectral Devices; SVM: support vector machine; VNIR: visible and near-infrared; VCA: vertex component analysis; REP: red edge position; ESAM: extended spectral angle mapping; HLB: huanglongbing; MS image: Multispectral image; ROI: region of interest; CFA Lab: colour feature analysis laboratory; KNN: K-nearest neighbours; LDA: linear discriminant analysis; SWIR: short-wave infrared; PCA: principal component analysis; QDA: quadratic discriminant analysis; NB: naïve bayes; BDT: binary decision tree; PLSR: partial least squares regression; ELM: extreme learning machine; BPNN: backpropagation neural network; PLS-DA: partial least squares discriminant analysis; EWS: early warning system; LS-SVM: least-squares support vector machine; NDVI: normalised difference vegetation index; GI: greenness index; ARI: anthocyanin reflectance index; RBF: radial basis function; CNN: convolutional neural network.

Support vector machine (SVM) is a usual technique for hyperspectral data analysis. It operates on the empirical risk minimisation principle which is effective at establishing class boundaries in high-dimensional feature spaces even when a limited amount of training data is available. Support vector machine is more effective regarding classification precision, processing speed and exhibit low sensitivity to the Huges phenomenon resulting in reducing the phase that takes a long time and is necessary for any other feature reduction technique (70). Application of SVM in foliar disease identification from hyperspectral data, identifies the initial symptoms even before they become apparent to the human eye (71).

Using both visible–near-infrared (VISNIR) and SWIR spectral ranges, linear discriminant analysis (LDA) is used to separate inoculated from uninoculated tomato leaves in hyperspectral imaging data as early as two hours after inoculation. Linear discriminant analysis consistently exhibited the best classification performance across all four bacterial leaf spot disease progression stages at the leaf level, while also providing interpretable visualisations through LDA plots that revealed clear spectral separation between healthy,

© The Author(s) 2026. Creative Commons CC BY 4.0. Published by Horizon e-Publishing Group.
https://doi.org/10.14719/pst.17031

bacterially infected and abiotically stressed leaf tissues. The LDA proves its effectiveness as both a classification and visualisation tool in pre-symptomatic plant disease detection (2).

A versatile ML technique called K-nearest neighbours (K-NN) is applied to both classification and regression issues. This algorithm is referred to as an instance-based algorithm, because instead of learning a model from training samples, all the training samples are stored in memory and predictions are made based on similarity assessment between a test sample and training samples (72).

extreme gradient boosting (XG Boost) is employed specifically for precise categorisation of plant diseases in pepper, tomato and potato crops along with convolutional neural networks (CNN) which extracts features from images (73).

Random forest (RF) is used in classifying healthy and infected vegetable leaves (brinjal, cluster beans, long beans) from hyperspectral reflectance data, where it creates multiple decision trees by randomly selecting samples and generates a separate tree for each sample. Each tree gives its own prediction (vote) and the final product is chosen from the class that gets the most votes, making it resistant to overfitting since no single tree dominates the final result (30). Modified random forest classifiers combined with LDA-reduced hyperspectral features were developed to detect and classify powdery mildew infection severity levels in Chardonnay grape bunches (39).

Decision tree model- bagged decision tree (BDT) is a non-linear classifier used for classifying into four categories: healthy, asymptomatic-infected, symptomatic-infected and freeze-damaged avocado leaves from VISNIR spectral data, where multiple classification trees are developed using bootstrap replicates (randomly resampled subsets of training data) to strengthen and stabilise the final classification. Its main advantage over a single decision tree is that the bagging (bootstrap aggregating) process lowers variance and overfitting, making it more robust and efficient for detecting laurel wilt even in asymptomatic leaves where spectral differences are minimal (74).

Regression models

Regression models generate continuous numerical outputs rather than fixed categories, making them well suited for tasks like measuring pigment concentrations or quantifying disease severity (15).

The frequent method employed to interpret hyperspectral images is partial- least square regression (PLSR) because it can handle a large number of highly correlated bands. The PLSR is used to manage a lot of bands that are highly connected. The degradation of carotenoids and chlorophyll caused by an angular leaf spot infection is measured using PLSR (75). Using hyperspectral reflectance data, the extent of damage caused by sclerotinia rot in celery was modelled using PLSR, which effectively managed the high-dimensional space of spectral data and multicollinearity of spectral bands. This model helped find significant wavelengths that were highly responsive to disease-induced physiological alterations in plant tissues for the prediction of disease extent based on hyperspectral imaging analysis (76).

Gaussian process regression (GPR), PLSR and v support vector regression (v-SVR) methods were employed in wheat leaf rust disease detection. The GPR outperformed both PLSR and SVR in detecting wheat leaf rust disease severity from hyperspectral data. All three ML regression techniques surpassed traditional spectral vegetation indices, indicating that ML methods are more effective for disease severity detection, especially when disease symptoms and varying training sample sizes are considered (76).

Unsupervised learning

Unsupervised methods find hidden patterns and connections within data and therefore fall under the category of pattern recognition (16).

Unsupervised ML (spectral unmixing, clustering and structure detection) was applied to classify hyperspectral images with low spatial resolution, proving that unsupervised approaches can effectively detect and classify surfaces without requiring labelled training data, offering a practical solution when ground truth information is unavailable in remote sensing applications (77).

K-means clustering was used as an unsupervised method to segment the leaf from the background in the hyperspectral images, by exploiting the unique spectral signature difference between vegetation and surrounding materials (soil, plastics, metals etc.). It classifies image spectra into two clusters (leaf and background), generating a 2D leaf mask to ensure only leaf spectral measurements were used for further disease classification (29).

Simplex volume maximisation (SiVM) was used as a data-driven, unsupervised matrix factorisation technique to automatically extract characteristic spectral signatures from hyperspectral microscopy data of barley leaves affected with powdery mildew (*Blumeria graminis*). The automated SiVM methodology produced results comparable to the labour-intensive and time-consuming manually assessed hyperspectral signatures, but it was assessed in a shorter period of time than traditional approaches. Additionally, it was employed to produce intuitive summaries of several barley genotypes, including fingerprints and traces of hyperspectral dynamics (78).

The unsupervised diffusion and volume-maximising interface segmentation (D-VIS) clustering algorithm efficiently divides hyperspectral image data into significant spectral classes by combining a volume-maximising geometric clustering technique with diffusion maps or nonlinear dimensionality reduction. This technique works completely without labelled training data, which makes it suitable for identifying minute spectral changes in complicated hyperspectral imaging that are linked to plant diseases like ash dieback (*Hymenoscyphus fraxineus*) (79).

© The Author(s) 2026. Creative Commons CC BY 4.0. Published by Horizon e-Publishing Group.
https://doi.org/10.14719/pst.17031

Application of six ML classifiers back propagation neural network (BPNN), extreme learning machine (ELM), least squares support vector machine (LS-SVM), SVM, random forest and partial least squares discriminant analysis (PLS-DA) on hyperspectral imaging data to pre-symptomatically detect tobacco mosaic virus (TMV) infection in tobacco leaves, where BPNN, ELM and LS-SVM outperformed others achieving up to 95 % accuracy via data fusion, enabling early detection as fast as 48 hr post-infection, far before visible symptoms appear (5–11 days), proving hyperspectral imaging with ML as a powerful non-invasive tool for precision agriculture (80).

Deep learning approaches in data analysis

Conventional ML approaches frequently rely on predetermined features, while deep learning models spontaneously uncover significant patterns and representations in data throughout the learning process to solve a given task. This makes deep learning suitable for analysing hyperspectral images with large datasets containing hundreds of spectral bands for detecting specific diseases. Deep learning approaches handle the challenges of hyperspectral data: higher dimensionality and limited labelled training data and automatically learn features without human guidance (16).

Non-imaging hyperspectral signatures of healthy and diseased (*S. tritici* and *S. nodorum*) wheat tissues were distinguished from each other by studying the red-edge reflectance patterns (705–745 nm) of the wheat. The high spectral variability was linked with the severity of the disease. A perceptron neural network was capable of correctly classifying 88–99 % of cases and predicted yield losses (35–45 % for severe STB, 20 –40 % for severe SNB). The results offer a fast, objective method for later-stage disease assessment and crop loss estimation in wheat in the field (20).

Application of back propagation neural networks (BNN) on second-derivative-transformed hyperspectral (VNIR/SWIR) data of oilseed rape leaves to classify *Alternaria* fungal infection, achieving 90.5 % accuracy for identifying days after inoculation and 80.5 % for distinguishing fungal species (81).

Artificial neural network (ANN)-based hyperspectral-based plant disease detection shows exceptional performance by providing near-perfect classification accuracy for presymptomatic oil palm disease by incorporating both spectral and weather data as model inputs. However, accuracy for the paired healthy class was as low as 66.7 % and the dataset had fewer than 50 spectral measurements per class, so this should be read as a preliminary, class-imbalanced result rather than a generalisable finding. Among the various ANN types evaluated, BPNN and extreme learning machine (ELM) were able to classify healthy versus diseased tobacco leaves with up to 95 % accuracy, while multilayer perceptron using multi-layer perceptron (MLP)-autoreggressive distributed lag (ARD) or automatic relevance determination and XY-fused networks (spectral (X) and spatial (F) information) were able to detect tomato chlorosis virus with over 85 % accuracy. These results collectively demonstrated ANN as a trusted and adaptable technique for early plant disease, through claims of perfect accuracy warrant scrutiny of sample size and validation design (9).

Automatic extraction of hierarchical spatial features from both hyperspectral and RGB images, CNNs have been used to detect yellow rust in wheat. This method offers superior classification accuracy by learning intricate spectral-spatial patterns across different stages of disease progression. The two hidden layer MLP utilising bayesian regularisation was implemented, incorporating spectral band data and lesion index as input features to effectively categorise wheat canopy into healthy or diseased classes (82).

Three dimensional (3D) deep convolutional neural network (3D-DCNN) extracts spatial and spectral features from hyperspectral image cubes to classify soybean stems as healthy or charcoal rot infected. A visualisation technique based on saliency maps is employed to determine the most sensitive pixel locations and hyperspectral wavelengths (particularly in the NIR region) that make significant contribution to classification accuracy (83, 84).

The outlier removal auxiliary classifier generative adversarial nets (OR-AC-GAN) model, which is based on generative adversarial nets (GAN), is an all-in-one framework that integrates spectrum classification, image classification and plant segmentation to detect tomato spotted wilt virus (TSWV) from hyperspectral images even before symptoms become apparent. The GAN model consists of two components: 1) the generator increases the quantity of the training dataset and enhances the precision of current disease detection techniques by producing artificial spectrum data that resembles real plant data. 2) the discriminator, which serves as a filter to reject inaccurate or noisy data, making sure that healthy plants are rarely mistakenly identified as unhealthy (85). Fig. 2 shows the overall process for hyperspectral-based plant disease detection.

Conventional ML classifiers (SVM, RF) are appropriate for specific, well-defined disease classifications because they often perform well on limited, carefully selected datasets and provide interpretability and minimal computational cost. On complicated, multi-class, or early-stage detection tasks, DL techniques (CNN, 3D-DCNN, GAN) perform better than ML; nevertheless, their field deployment in data-scarce crop systems is limited because they require larger labelled datasets and more processing power.

Applications of hyperspectral technology in plant disease diagnosis

Plant disease diagnosis mainly involves detection, differentiation, identification, evaluation of disease severity and evaluation of genotype resistance. These are carried out using corresponding measurement scales at various levels of biological organisation. In laboratories, hyperspectral microscopes are used to

© The Author(s) 2026. Creative Commons CC BY 4.0. Published by Horizon e-Publishing Group.
https://doi.org/10.14719/pst.17031

observe fungal spores and identify metabolic alterations brought on by plant-pathogen interactions at the cellular and tissue levels.

These studies are mainly conducted for fundamental research, pathogen identification and genotype resistance evaluation. At the individual organ level (such as leaves, stems, roots, fruits and ears) and the whole-plant level, hyperspectral measurements are conducted in laboratories, greenhouses and field settings to enable early disease detection and differentiation. Hyperspectral technologies are widely applied for large-scale disease mapping and field conditions to enable early disease detection and differentiation at the canopy level. Research has shown that hyperspectral technologies are useful for diagnosing plant diseases in these many application areas (14). Fig. 3 illustrates the major applications, spatial scales and acquisition environments associated with hyperspectral remote sensing for plant disease diagnosis. Fig. 3 illustrates the major applications, spatial scales and acquisition environments associated with hyperspectral remote sensing for plant disease diagnosis.

Disease detection

Differentiating healthy plants from diseased ones is the primary objective of disease detection. Here, the study concentrates on a single, particular illness, including its symptoms and progression. Time-series data based on infrared thermography, chlorophyll fluorescence imaging and hyperspectral imaging were compared under controlled conditions in the study on fusarium head blight in wheat. As early as the third day following inoculation, fusarium-infected and non-inoculated spikelets could be identified using a pigment-specific simple ratio derived from hyperspectral imaging, with an SVM model classification accuracy of 78 % (86).

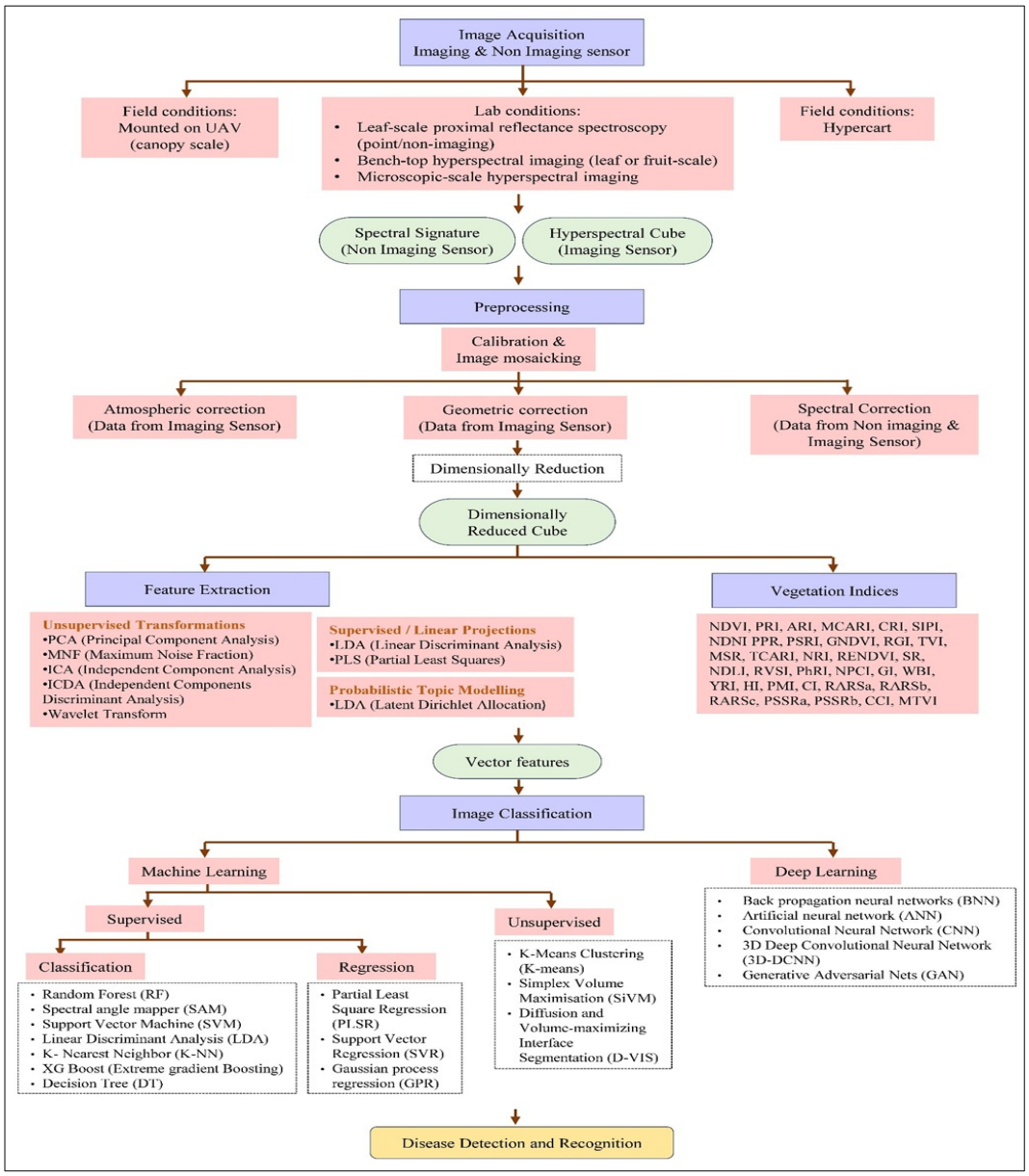


Fig. 2. Generalised approach for hyperspectral-based plant disease detection.

© The Author(s) 2026. Creative Commons CC BY 4.0. Published by Horizon e-Publishing Group.
https://doi.org/10.14719/pst.17031

Similar to this, citrus canker was detected at asymptomatic, early and late disease phases using a hyperspectral imaging system (400–1000 nm). The k-nearest neighbour (KNN) approach was outperformed by the radial basis function (RBF) classifier, which attained overall accuracy of 94 and 96. When the same technology was mounted on a UAV, it was able to differentiate between healthy and canker-infected trees with near-perfect classification accuracy. However, the result came from a small orchard trial (four trees, 20 spectrally correlated regions of interest sampled per tree canopy in the field and evaluated with an internal 70/20/10 split rather than independent validation), so the perfect accuracy should be read as preliminary, not as confirmation of a generalisable method (66, 87). *Burkholderia cepacia*-caused sour skin disease in onions was reliably recognised using a SWIR camera with PCA and Fisher's discriminant analysis (FDA) (22).

Disease identification and differentiation

Determining a specific pathogen that is damaging the plant and differentiating between other diseases is the goal of disease identification. Specific spectral indices were developed for differentiating three diseases in sugarbeet: Powdery mildew, sugar beet rust and *Cercospora* leaf spot. Using the RELIEF-F algorithm to extract key wavelength (450–950) healthy and diseased leaves were classified with balanced classification accuracies of 89, 92, 87 and 85 % respectively (53). Brown rust (*Puccinia triticina*) and yellow rust (*P. striiformis*) on wheat leaves can be distinguished from one another. To identify the spectral signal of rust spores in mixed spectra, hyperspectral images were subjected to least-squares factorisation (18).

Disease severity assessment

One of the most important applications of hyperspectral technology is the quantitative determination of plant disease severity. The spatial distribution of chlorophyll and carotenoid levels in angular leaf spot-affected cucumber leaves is mapped using hyperspectral imaging. Partial least square regression (PLSR) models were applied pixel-by-pixel to the hyperspectral images in order to quantify the relationship between pigment concentrations and disease severity in spectra data (75). For wheat powdery mildew, hyperspectral reflectance of healthy and infected leaves is measured and 32 spectral features are extracted. The PLSR model surpasses the multivariate linear regression model, yielding a relative root mean square error of 0.23 and a coefficient of determination of 0.80 utilising seven specified spectral indices (88). In potato, late blight severity assessment was effectively carried out using UAV-based hyperspectral imaging and simplex volume maximisation (SiVM) (23).

Assessment of genotype resistance

In plant breeding, pathogen-host interactions are essential for determining many genotypes' resistance to a certain disease. Plant genotype phenotyping is primarily accomplished through labour-intensive and expensive visual evaluations in conventional breeding techniques. In this regard, hyperspectral analysis offers a practical non-invasive alternative for automating and speeding up traditional phenotyping techniques. Five sugar beetroot genotypes' susceptibility to *Cercospora* leaf spot was tested using a mix of hyperspectral and conventional methods. It was discovered that the amount of pathogen spores and their spatial distribution determined the spectral properties of affected leaf areas, with resistant plants having less conidia per infected leaf area. A useful technique for identifying minute variations in genotype resistance was found to be hyperspectral imaging of lesion morphologies with regard to sporulation (89). At the microscopic scale, a hyperspectral microscope is used to determine barley cultivar resistance to powdery mildew (*Blumeria graminis*). Daily recordings showed that susceptible genotypes exhibited increased reflectance in the visible range as symptoms developed, whereas the spectral signature of resistant genotypes showed no significant changes throughout the experimental period (78).

Integration with other remote sensing technologies

Hyperspectral + LiDAR

An UAV study on pine wilt disease showed that hyperspectral alone outperformed LiDAR alone but their combination gave best classification accuracy with LiDAR crown metrics essential for distinguishing dead trees while hyperspectral features contributed most overall. The UAV-based system that combines LiDAR and hyperspectral sensors has a great chance of identifying pine wilt disease early on and preventing its spread before an outbreak occurs (90).

Hyperspectral + thermal

The integration of thermal infrared (TIR) imagery and hyperspectral reflectance provides complementary biochemical and physiological disease signals. Thermal data capture canopy temperature anomalies caused by pathogen-induced vascular disruption and stomatal closure, while hyperspectral data records pigment degradation, water content shifts and fluorescence emission. This enables pre-symptomatic detection much in advance of the onset of visual symptoms. Combining a 3-D radiative transfer model with high-resolution hyperspectral (VNIR and SWIR) and thermal imaging, more than 1,100 holm oak trees affected by *Phytophthora cinnamomi* in Spain were detected. Canopy temperature emerged as the most diagnostically significant variable and retrieved plant functional traits successfully detected disease in 34 % of visually asymptomatic trees, indicating that thermal data are the first and most sensitive markers of sub-visual decline and that pathogen-induced physiological deterioration occurs before any detectable leaf pigment or canopy structural modification (91).

Hyperspectral + multispectral + thermal

Remote sensing technologies are used to identify vascular diseases brought on by the pathogens *Verticillium dahliae* and *Xylella fastidiosa* in almond and olive trees. Hyperspectral and thermal datasets are

© The Author(s) 2026. Creative Commons CC BY 4.0. Published by Horizon e-Publishing Group.
https://doi.org/10.14719/pst.17031

compared with high-resolution multispectral satellite images from WorldView-2 and -3 to determine their effectiveness across different stages of disease progression. Since both pathogens are vascular in nature, water stress is a key symptom making thermal data through the crop water stress index (CWSI) a valuable addition to improve detection. Multispectral sensors lack the spectral bands necessary for early-stage disease detection, where indices such as anthocyanins, solar-induced fluorescence, blue NPQI and PRIn are crucial, making hyperspectral data vital for comprehensive disease monitoring. Commercial multispectral imagery can effectively detect intermediate and advanced diseases caused by these vascular infections (92).

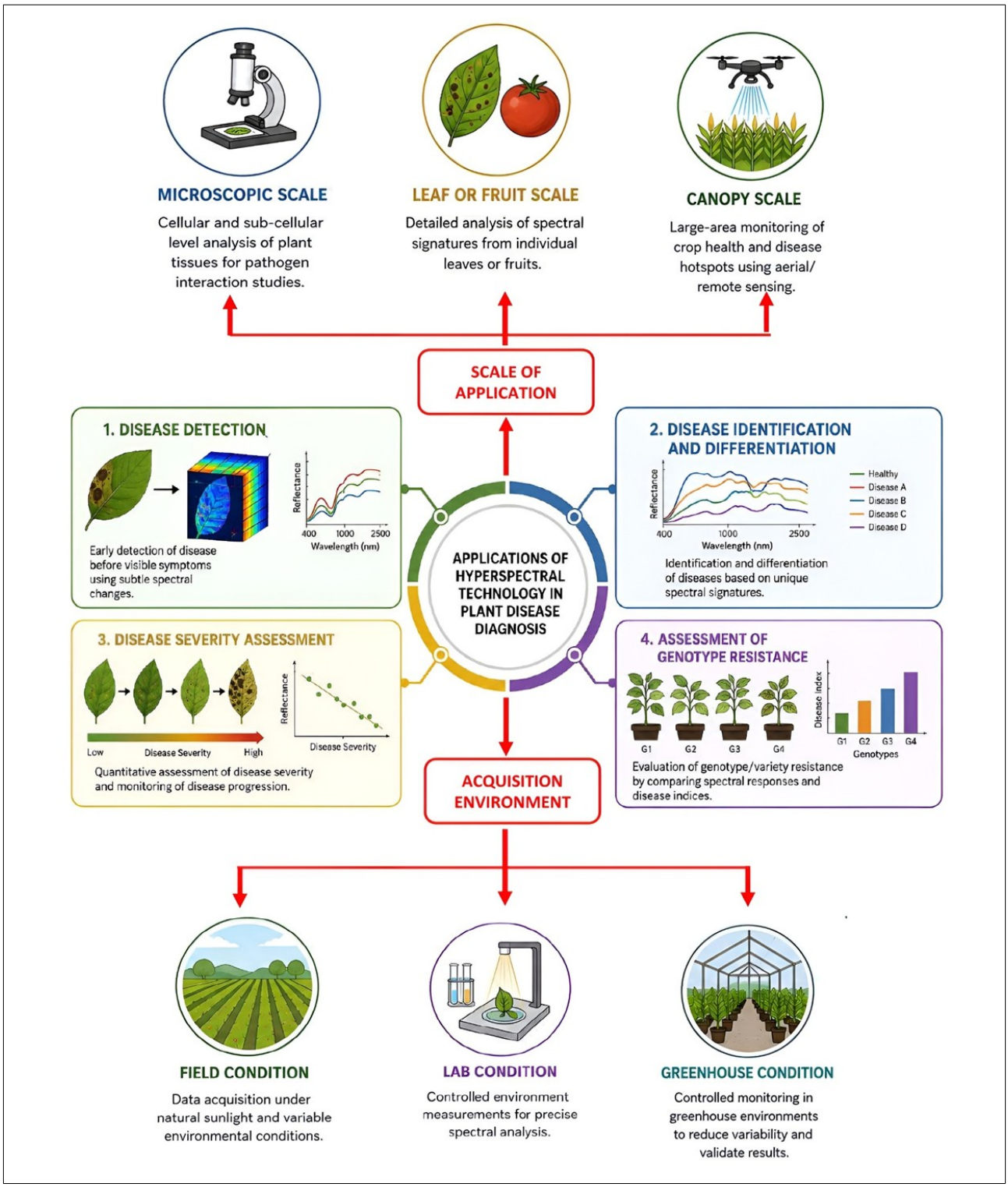


Fig. 3. Conceptual framework of hyperspectral technology applications across spatial scales and acquisition environments for plant disease diagnosis.

© The Author(s) 2026. Creative Commons CC BY 4.0. Published by Horizon e-Publishing Group.
https://doi.org/10.14719/pst.17031

Hyperspectral + red, green and blue + thermal

Monitoring wheat powdery mildew using three different data sources: RGB, thermal infrared and hyperspectral imaging data. Ten disease-sensitive VIs are calculated using hyperspectral data; RGB images are processed to extract texture features (TF) using a gray-level co-occurrence matrix; and thermal infrared imagery provides canopy temperature parameters (TP) such as the canopy temperature difference and normalised relative canopy temperature. The main idea is that the accuracy and robustness of disease index prediction are greatly enhanced by combining data from multiple sources, which combines spectral, textural and thermal information, even if each data source alone, especially VIs, offers predictive ability (93).

Challenges and limitations

Hyperspectral technologies have shown considerable promise in controlled research settings, but the transition to real-world agricultural use remains incomplete. In order to monitor canopy-based vegetation indices in low-altitude agricultural production, airborne and satellite multispectral systems are currently frequently used (37). However, precise remote sensing monitoring of plant diseases is typically only feasible when symptoms are completely apparent, which may be too late for disease control. Despite significant scientific developments in the use of hyperspectral sensors for early plant disease diagnosis, its practical deployment in field and greenhouse settings in precision farming systems is still a hurdle.

A major technical barrier lies in the stark difference between laboratory and field lighting environments. In the majority of controlled experiments, artificial illumination was used to precisely control the directions of incoming light and reflected light being caught by positioning the camera or sensor at a specific angle to the leaf tissue. The canopy conditions in the real world vary greatly; areas with direct sunlight seem noticeably brighter than shaded layers; tissue colour changes according to the angle of incoming and outgoing light; and image brightness heterogeneities fluctuate minute by minute. The overall brightness of the specific image within the position and angle of incidence of light must therefore be taken into account when defining a threshold for distinguishing between healthy and diseased tissue, which remains a challenge (94, 95).

The accurate identification of a particular disease under realistic field settings when several crop stressors are present simultaneously is another unsolved problem. These days, most monitoring studies and applications are carried out in experimental fields or areas where the type of disease is already known. It is challenging to achieve a reliable and accurate monitoring result in a region without appropriate data. Furthermore, separation is particularly difficult because many pathogen and abiotic stresses induce comparable visual symptoms and, as a result, similar spectral signatures.

Deep learning algorithms and other sophisticated computer techniques were crucial in distinguishing between biotic and abiotic stresses in field and greenhouse settings (96, 97). However, these tools are not yet full-fledged for widespread practical use. Encouraging the development of a knowledge base with background information on diseases (such as geographic distribution, favourable habitats, soil types and climate conditions) is also crucial. Although it is currently unavailable at the scale necessary for widespread deployment, such prior knowledge might greatly reduce uncertainty in disease monitoring.

While many minor and regionally significant crops, along with co-occurring or complex disease interactions, remain largely unstudied despite their significance for regional food security, research effort is still focused on a small number of high-value crops (wheat, rice, tomato) and well-characterised diseases. Furthermore, the majority of research assumes that each plant has a single pathogen, which usually ignores the detection of concurrent or overlapping biotic and abiotic stresses.

Most studies employ staged illumination, single-leaf imaging and controlled lab or greenhouse conditions to claim accuracies that do not account for field-level variability like weather, canopy overlap, fluctuating light and background noise. Although this controlled setup is helpful for isolating disease-specific spectral signals, the high reported accuracies might not hold up in real-world field conditions with more environmental noise. This underscores the need for additional field-validated studies before such systems can be regarded as deployment-ready.

Future perspectives

Real field dataset testing

Instead of mainly depending on public or lab datasets, models must be trained and validated on images captured from actual field conditions across the crop life cycle (98).

High-performance deep learning approaches

The limitation of current CNN models urges the development of more advanced architectures, which enable earlier and accurate disease identification across multiple crop species. Developing a unified CNN model which is essential for classifying multiple disease types across multiple crop species instead of creating a distinct model for each class (98). Future research should focus on developing deep learning algorithms that are robust under natural field illumination and capable of distinguishing overlapping biotic and abiotic stress symptoms. These algorithms should be supported by comprehensive disease knowledge bases, including geographical distribution, habitats, soil and climate data to minimise monitoring uncertainty (14, 15).

© The Author(s) 2026. Creative Commons CC BY 4.0. Published by Horizon e-Publishing Group.
https://doi.org/10.14719/pst.17031

Recognise complex disease patterns

Models should handle more complex and visually similar disease symptoms that current models struggle to differentiate using hyperspectral data. Broader neural network applications -expanding DL applications to identify a wider range of diseases and stress conditions where neural networks are not yet fully investigated (98).

Lab to field performance gap

Models show drastic accuracy drops when moving from controlled to real-world datasets. This trend is exhibited across all architectures indicating the problem is systematic, not model-specific. Current research tends to focus on optimising laboratory accuracy before considering real-world deployment needs. A more effective approach would embed practical implementation requirements into the design process from the very beginning of development stages. One important area of research is resource-efficient optimisation, which focuses on architectures that retain field accuracy above 80 % while obtaining inference times under 100 ms and model sizes under 5 MB (99). Advances hinge on combining higher resolution pathogen-scale identification with auxiliary data for biotic/abiotic stress discrimination, developing multisource early warning systems (VIS-SWIR, fluorescence, thermal, SAR, LIDAR) for field-scale detection during the incubation period, the expansion of spaceborne hyperspectral missions with a unified plant-disease spectral library to enable joint ground-airborne-spaceborne monitoring at regional and global scales (1, 18).

Adaptive complexity systems and cost-effective design

Adaptive complexity approach is another promising research direction, as it involves designing models to automatically adjust their computational requirements depending on the computing resources that are available to support their execution. Economic feasibility needs to become one of the central considerations in addition to traditional technical criteria used for evaluating computer technologies. Real-world case studies reveal that those computer systems that give preference to convenience and cost-effectiveness over utmost precision in their results prove to be the most efficient. This ensures that economic factors play a central role in modifying architectural design decisions, creating greater adoption and more successful application in practical settings (99). Future development should integrate advanced machine learning with hyperspectral data processing while incorporating on-chip real-time computation systems (e.g., FPGA) so plant disease identification models can support real-time field control strategies (35).

Generalisation across agricultural regions

The need for improved generalisation techniques is highlighted by the 40–60 % performance differences that agricultural AI systems currently exhibit across different climatic zones. By allowing cooperative model training across regions while protecting data privacy and local governance, federated learning presents a viable option that could lower geographic performance variation to less than 10 %. In addition, few-shot learning allows models to quickly adapt to new environments using fewer than 100 training samples with transformer-based models. Furthermore, climate-aware domain adaptation includes environmental factors into model architectures, helping systems account for seasonal and regional differences in disease presentation and improving overall detection reliability across diverse agricultural contexts (99).

Temporal monitoring systems

Temporal monitoring allows for additional research opportunities to be gained through processes which allow for the tracking of the disease's development process rather than offering single time detection results. Incorporating predictive disease modelling guides on delivering the treatment at the right time and place, such as longitudinal monitoring that enables precision intervention strategies, possibly enhancing agricultural results and resource effectiveness in disease control techniques (99).

Bias detection and mitigation

Implementing agricultural AI in an ethical and equitable manner requires careful consideration of a number of factors. Bias detection and mitigation are basic issues that necessitate more inclusive data collection methods because existing datasets exhibit notable disparities in representation across socioeconomic and geographic contexts that could be detrimental to particular agricultural methods, localities, or crop varieties. Establishing suitable risk management techniques and decision thresholds across various farming scales requires an understanding of the impact of diagnostic errors, where false positives lead to needless treatments and false negatives permit unchecked disease progression (99).

Seedborne pathogen detection

Future research will concentrate on standardising techniques and testing spectral signatures for contaminated seed identification. Hyperspectral imaging in conjunction with AI is a promising area for seedborne pathogen detection. While the non-destructive nature of HSI enables the screening of every seed without sample destruction, epidemiological studies that connect spectral data to disease outbreaks will aid in the establishment of acceptable contamination thresholds. Combining HSI with existing molecular methods will further enhance detection reliability and specificity (100). Strong interdisciplinary cooperation between plant pathologists, engineers, physicists and software experts is necessary to advance this technology (9). Despite challenges related to high equipment cost and the need for cross-disciplinary teamwork, HSI is expected to greatly benefit seed certification programmes and strengthen farmer confidence by enabling large-scale screening for critical seedborne pathogens (100).

© The Author(s) 2026. Creative Commons CC BY 4.0. Published by Horizon e-Publishing Group.
https://doi.org/10.14719/pst.17031

The integration of HSI with more comprehensive AI-driven decision-support systems will be crucial to its future development in precision agriculture. This integration will go beyond disease diagnosis to provide practical, farm-level management advice. They also highlight the increasing convergence of digital agriculture infrastructure, including Internet of Things (IoT)-based sensor networks and automated data pipelines, with hyperspectral sensing as a crucial path for expanding these technologies outside of regulated research environments. However, specific emerging concepts like fully automated IoT-integrated monitoring systems, digital twins for real-time crop simulation and hyperspectral-informed climate change adaptation strategies remain largely undeveloped in the current literature, offering significant open avenues for future research and practical deployment (12).

Conclusion

Plant disease detection using hyperspectral remote sensing has become a ground-breaking technology with superior spectral discrimination capabilities that enable early presymptomatic disease detection and continuous monitoring and overcome the limitations of traditional multispectral approaches. The synergistic integration of spectral signatures with advanced feature extraction, dimensionality reduction techniques and vegetation indices has improved accuracy and consistency of automated disease detection. Machine learning (ML) and deep learning approaches have greatly improved disease classification and diagnosis. Emerging deep learning models eliminate the need for manual feature selection and increase classification accuracy by automatically extracting features from hyperspectral data. These techniques effectively detect subtle spectral changes in the early infection stage, supporting early warning systems in precision agriculture. Disease monitoring is strengthened when hyperspectral data are integrated with other complementary remote sensing technologies like multispectral sensors, thermal sensors, LiDAR and unmanned aerial vehicle (UAV) systems. Each technology contributes unique information: thermal data detects stress-related temperature changes, LiDAR measures canopy structural changes and UAVs provide frequent high-resolution data collection. These integrated approaches facilitate comprehensive, multi-dimensional crop health assessment. Thus, hyperspectral remote sensing provides farmers with a practical pathway to early, non-destructive disease identification, enabling timely intervention that lowers input costs and protects crop yield and income. Development of efficient algorithms for real-time monitoring, cloud-based analytical platforms, reduced sensor costs and enhanced data fusion will drive the transition of hyperspectral remote sensing from research applications to operational agricultural systems, establishing it as a cornerstone technology for precision agriculture and sustainable disease management.

Acknowledgements

The authors would like to thank the Department of remote Sensing and GIS, Tamil Nadu Agricultural University for providing the necessary computational resources and intellectual support throughout the development of this review article. The authors are grateful to colleagues and reviewers for their insightful feedback and suggestions that enhanced the quality of the manuscript.

Authors' contributions

VS conducted an extensive literature review and contributed to the overall framework and conceptualisation of manuscript as well, as assisting in the preparation of tables and figures. KR supervised the review, provided critical insights to the manuscripts, reviewed and edited all sections to ensure coherence and quality. JR prepared supplementary materials and assisted in the final proof reading of the manuscript. The review was further edited by SK, KS, NRM and SDSJ. All authors have read and approved the final manuscript.

Compliance with ethical standards

Conflict of interest

Authors do not have any conflict of interests to declare.

Ethical issues

None

Declaration of generative AI and AI-assisted technologies in the writing process

During the preparation of this work, the authors used Claude AI to enhance language clarity and image modification. After using this tool/service, the authors reviewed and edited the content as needed and takes full responsibility for the publication's content.

References

1. Zhang N, Yang G, Pan Y, Yang X, Chen L, Zhao C. A review of advanced technologies and development for hyperspectral-based plant disease detection in the past three decades. Remote Sens. 2020;12(19):3188. https://doi.org/10.3390/rs12193188
2. Zhang X, Vinatzer BA, Li S. Hyperspectral imaging analysis for early detection of tomato bacterial leaf spot disease. Sci Rep. 2024;14(1):27666. https://doi.org/10.1038/s41598-024-78650-6
3. Lowe A, Harrison N, French AP. Hyperspectral image analysis techniques for the detection and classification of the early onset of plant disease and stress. Plant Methods. 2017;13(1):80. https://doi.org/10.1186/s13007-017-0233-z

© The Author(s) 2026. Creative Commons CC BY 4.0. Published by Horizon e-Publishing Group.
https://doi.org/10.14719/pst.17031

4. Gaikwad A, Kharbadkar V. Hyperspectral imaging: a tool for plant disease detection. Agri Articles. 2024;4(01):192–8. https://doi.org/10.13140/RG.2.2.23479.09129
5. Mishra P, Lohumi S, Khan HA, Nordon A. Close-range hyperspectral imaging of whole plants for digital phenotyping: recent applications and illumination correction approaches. Comput Electron Agric. 2020;178:105780. https://doi.org/10.1016/j.compag.2020.105780
6. García-Vera YE, Polochè-Arango A, Mendivelso-Fajardo CA, Gutiérrez-Bernal FJ. Hyperspectral image analysis and machine learning techniques for crop disease detection and identification: a review. Sustainability. 2024;16(14):6064. https://doi.org/10.3390/su16146064
7. Singh R, Gehlot A, Prajapat MK, Singh B. Artificial intelligence in agriculture. Boca Raton: CRC Press; 2021. https://doi.org/10.1201/9781003245759
8. Nyawose T, Maswanganyi RC, Khumalo P. A review on the detection of plant disease using machine learning and deep learning approaches. J Imaging. 2025;11(10):326. https://doi.org/10.3390/jimaging11100326
9. Terentev A, Dolzhenko V, Fedotov A, Eremenko D. Current state of hyperspectral remote sensing for early plant disease detection: a review. Sensors. 2022;22(3):757. https://doi.org/10.3390/s22030757
10. Wieme J, Mollazade K, Malounas I, Zude-Sasse M, Zhao M, Gowen A, et al. Application of hyperspectral imaging systems and artificial intelligence for quality assessment of fruit, vegetables and mushrooms: a review. Biosyst Eng. 2022;222:156–76. https://doi.org/10.1016/j.biosystemseng.2022.07.013
11. Franke J, Menz G, Oerke EC, Rascher U, editors. Comparison of multi- and hyperspectral imaging data of leaf rust infected wheat plants. In: Remote sensing for agriculture, ecosystems and hydrology VII. Bellingham (WA): SPIE; 2005. https://doi.org/10.1117/12.626531
12. Ram BG, Oduor P, Igathinathane C, Howatt K, Sun X. A systematic review of hyperspectral imaging in precision agriculture: analysis of its current state and future prospects. Comput Electron Agric. 2024;222:109037. https://doi.org/10.1016/j.compag.2024.109037
13. Wu D, Sun DW. Advanced applications of hyperspectral imaging technology for food quality and safety analysis and assessment: a review-Part I: fundamentals. Innov Food Sci Emerg Technol. 2013;19:1–14. https://doi.org/10.1016/j.ifset.2013.04.014
14. Cheshkova A. A review of hyperspectral image analysis techniques for plant disease detection and identification. Vavilovskii Zhurnal Genetiki i Selektsii. 2022;26:202–13. https://doi.org/10.18699/VJGB-22-25
15. Thomas S, Kuska MT, Bohnenkamp D, Brugger A, Alisaac E, Wahabzada M, et al. Benefits of hyperspectral imaging for plant disease detection and plant protection: a technical perspective. J Plant Dis Prot. 2018;125(1):5–20. https://doi.org/10.1007/s41348-017-0124-6
16. Mahlein AK, Kuska MT, Behmann J, Polder G, Walter A. Hyperspectral sensors and imaging technologies in phytopathology: state of the art. Annu Rev Phytopathol. 2018;56:535–58. https://doi.org/10.1146/annurev-phyto-080417-050100
17. Couture J, Singh A, Charkowski A, Groves R, Gray S, Bethke P, et al. Integrating spectroscopy with potato disease management. Plant Dis. 2018;102(11):2233–40. https://doi.org/10.1094/PDIS-01-18-0054-RE
18. Bohnenkamp D, Kuska M, Mahlein AK, Behmann J. Hyperspectral signal decomposition and symptom detection of wheat rust disease at the leaf scale using pure fungal spore spectra as reference. Plant Pathol. 2019;68(6):1188–95. https://doi.org/10.1111/ppa.13020
19. Burkart A, Aasen H, Alonso L, Menz G, Bareth G, Rascher U. Angular dependency of hyperspectral measurements over wheat characterized by a novel UAV based goniometer. Remote Sens. 2015;7(1):725–46. https://doi.org/10.3390/rs70100725
20. Zhelezova SV, Pakholkova EV, Veller VE, Voronov MA, Stepanova EV, Zhelezova AD, et al. Hyperspectral non-imaging measurements and perceptron neural network for pre-harvesting assessment of damage degree caused by *Septoria/Stagonospora* blotch diseases of wheat. Agronomy.2023;13(4):1045. https://doi.org/10.3390/agronomy13041045
21. Mahlein AK, Steiner U, Hillnhütter C, Dehne HW, Oerke EC. Hyperspectral imaging for small-scale analysis of symptoms caused by different sugar beet diseases. Plant Methods. 2012;8(1):3. https://doi.org/10.1186/1746-4811-8-3
22. Wang W, Li C, Tollner EW, Gitaitis RD, Rains GC. Shortwave infrared hyperspectral imaging for detecting sour skin (*Burkholderia cepacia*)-infected onions. J Food Eng. 2012;109(1):38–48. https://doi.org/10.1016/j.jfoodeng.2011.10.001
23. Franceschini MHD, Bartholomeus H, Van Apeldoorn DF, Suomalainen J, Kooistra L. Feasibility of unmanned aerial vehicle optical imagery for early detection and severity assessment of late blight in potato. Remote Sens. 2019;11(3):224. https://doi.org/10.3390/rs11030224
24. Aasen H, Burkart A, Bolten A, Bareth G. Generating 3D hyperspectral information with lightweight UAV snapshot cameras for vegetation monitoring: from camera calibration to quality assurance. ISPRS J Photogramm Remote Sens. 2015;108:245–59. https://doi.org/10.1016/j.isprsjprs.2015.08.002
25. Fischer C, Kakoulli I. Multispectral and hyperspectral imaging technologies in conservation: current research and potential applications. Stud Conserv. 2006;51(Suppl 1):3–16.
26. Van De Vijver R, Mertens K, Heungens K, Somers B, Nuyttens D, Borra-Serrano I, et al. In-field detection of *Alternaria solani* in potato crops using hyperspectral imaging. Comput Electron Agric. 2020;168:105106. https://doi.org/10.1016/j.compag.2019.105106
27. Mishra P, Asaari MSM, Herrero-Langreo A, Lohumi S, Diezma B, Scheunders P. Close range hyperspectral imaging of plants: a review. Biosyst Eng. 2017;164:49–67. https://doi.org/10.1016/j.biosystemseng.2017.09.009
28. Zhang J, Huang Y, Pu R, Gonzalez-Moreno P, Yuan L, Wu K, et al. Monitoring plant diseases and pests through remote sensing technology: a review. Comput Electron Agric.2019;165:104943. https://doi.org/10.1016/j.compag.2019.104943
29. Moghadam P, Ward D, Goan E, Jayawardena S, Sikka P, Hernandez E, editors. Plant disease detection using hyperspectral imaging. 2017 International Conference on Digital Image Computing: Techniques and Applications (DICTA);2017. https://doi.org/10.1109/DICTA.2017.8227476
30. Ghule A, Deshmukh R, Gaikwad C. Distinguishing healthy and infected vegetable crops using hyperspectral leaf reflectance. CSI J. 2020;42.
31. Cozzolino D, Williams P, Hoffman L. An overview of pre-processing methods available for hyperspectral imaging applications. Microchem J. 2023;193:109129. https://doi.org/10.1016/j.microc.2023.109129
32. Dombi J, Dineva A. Adaptive Savitzky-Golay filtering and its applications. Int J Adv Intell Paradigms. 2020;16(2):145–56. https://doi.org/10.1504/IJAIP.2020.107011
33. Vidal M, Amigo JM. Pre-processing of hyperspectral images: essential steps before image analysis. Chemom Intell Lab Syst.2012;117:138–48. https://doi.org/10.1016/j.chemolab.2012.05.009

© The Author(s) 2026. Creative Commons CC BY 4.0. Published by Horizon e-Publishing Group.
https://doi.org/10.14719/pst.17031

34. Chaitra H, Kumar CM, Sharathchandra R, Narayanan P, Nidamanuri RR. Machine learning-based detection of fusarium wilt in tomato using ground-based and satellite hyperspectral imagery. Adv Space Res. 2026. https://doi.org/10.1016/j.asr.2026.03.018
35. Wan L, Li H, Li C, Wang A, Yang Y, Wang P. Hyperspectral sensing of plant diseases: principle and methods. Agronomy.2022;12(6):1451. https://doi.org/10.3390/agronomy12061451
36. Zhang J, Yang C, Zhao B, Song H, Clint Hoffmann W, Shi Y, et al. Crop classification and LAI estimation using original and resolution-reduced images from two consumer-grade cameras. Remote Sens. 2017;9(10):1054. https://doi.org/10.3390/rs9101054
37. Huang Y, Thomson SJ, Hoffmann WC, Lan Y, Fritz BK. Development and prospect of unmanned aerial vehicle technologies for agricultural production management. Int J Agric Biol Eng. 2013;6(3):1–10.
38. Cui B, Ma X, Xie X, Ren G, Ma Y. Classification of visible and infrared hyperspectral images based on image segmentation and edge-preserving filtering. Infrared Phys Technol.2017;81:79–88. https://doi.org/10.1016/j.infrared.2016.12.010
39. Knauer U, Matros A, Petrovic T, Zanker T, Scott ES, Seiffert U. Improved classification accuracy of powdery mildew infection levels of wine grapes by spatial-spectral analysis of hyperspectral images. Plant Methods. 2017;13(1):47. https://doi.org/10.1186/s13007-017-0198-y
40. Villa A, Benediktsson JA, Chanussot J, Jutten C. Hyperspectral image classification with independent component discriminant analysis. IEEE Trans Geosci Remote Sens.2011;49(12):4865–76. https://doi.org/10.1109/TGRS.2011.2153861
41. Shi X, Sun L, editors. Hyperspectral image classification with support vector machines based on the maximum noise fraction. 2022 IEEE 5th International Conference on Electronics Technology (ICET); 2022. https://doi.org/10.1109/ICET55676.2022.9824122
42. Shambulinga M, Sadashivappa G. Supervised hyperspectral image classification using SVM and linear discriminant analysis. Int J Adv Comput Sci Appl. 2020;11(10). https://doi.org/10.14569/IJACSA.2020.0111050
43. Zapolska A, Kalaitzidis C, Markakis E, Ligoxigakis E, Koubouris G. Linear discriminant analysis of spectral measurements for discrimination between healthy and diseased trees of *Olea europaea* L. artificially infected by *Fomitiporia mediterranea*. Int J Remote Sens. 2020;41(14):5388–98. https://doi.org/10.1080/01431161.2020.1731931
44. Lapajne J, Knapič M, Žibrat U. Comparison of selected dimensionality reduction methods for detection of root-knot nematode infestations in potato tubers using hyperspectral imaging. Sensors. 2022;22(1):367. https://doi.org/10.3390/s22010367
45. Phadikar S, Goswami J, editors. Vegetation indices based segmentation for automatic classification of brown spot and blast diseases of rice. 2016 3rd International Conference on Recent Advances in Information Technology (RAIT); 2016. https://doi.org/10.1109/RAIT.2016.7507917
46. Blei DM. Probabilistic topic models. Commun ACM. 2012;55(4):77–84. https://doi.org/10.1145/2133806.2133826
47. Wahabzada M, Mahlein AK, Bauckhage C, Steiner U, Oerke EC, Kersting K. Plant phenotyping using probabilistic topic models: uncovering the hyperspectral language of plants. Sci Rep. 2016;6(1):22482. https://doi.org/10.1038/srep22482
48. Serrano L, Peñuelas J, Ustin SL. Remote sensing of nitrogen and lignin in Mediterranean vegetation from AVIRIS data: decomposing biochemical from structural signals. Remote Sens Environ. 2002;81(2–3):355–64. https://doi.org/10.1016/S0034-4257(02)00011-1
49. Panigrahi B, Kathala KCR, Sujatha M. A machine learning-based comparative approach to predict the crop yield using supervised learning with regression models. Procedia Comput Sci. 2023;218:2684–93. https://doi.org/10.1016/j.procs.2023.01.241
50. Li H, Lee WS, Wang K, Ehsani R, Yang C. 'Extended spectral angle mapping (ESAM)' for citrus greening disease detection using airborne hyperspectral imaging. Precis Agric. 2014;15(2):162–83. https://doi.org/10.1007/s11119-013-9325-6
51. Meena SV, Dhaka VS, Sinwar D, editors. Exploring the role of vegetation indices in plant diseases identification. 2020 Sixth International Conference on Parallel, Distributed and Grid Computing (PDGC); 2020. https://doi.org/10.1109/PDGC50313.2020.9315814
52. Rumpf T, Mahlein A, Dörschlag D, Plümer L, editors. Identification of combined vegetation indices for the early detection of plant diseases. Remote Sensing for Agriculture, Ecosystems and Hydrology XI; 2009. https://doi.org/10.1117/12.830525
53. Mahlein A-K, Rumpf T, Welke P, Dehne H-W, Plümer L, Steiner U, et al. Development of spectral indices for detecting and identifying plant diseases. Remote Sens Environ.2013;128:21–30. https://doi.org/10.1016/j.rse.2012.09.019
54. Atanasov AI, Atanasov AZ, Evstatiev BI. Application of NDVI for early detection of yellow rust (*Puccinia striiformis*). AgriEngineering.2025;7(5):160. https://doi.org/10.3390/agriengineering7050160
55. Gamon JA, Penuelas J, Field C. A narrow-waveband spectral index that tracks diurnal changes in photosynthetic efficiency. Remote Sens Environ. 1992;41(1):35–44. https://doi.org/10.1016/0034-4257(92)90059-S
56. Sapate NM, Deshmukh RR. Spectral and numerical analysis of hyperspectral data using vegetation indices. Int J Eng Adv Technol. 2019;8. https://doi.org/10.35940/ijeat.F8578.088619
57. Guo A, Huang W, Dong Y, Ye H, Ma H, Liu B, et al. Wheat yellow rust detection using UAV-based hyperspectral technology. Remote Sens. 2021;13(1):123. https://doi.org/10.3390/rs13010123
58. Haboudane D, Miller JR, Pattey E, Zarco-Tejada PJ, Strachan IB. Hyperspectral vegetation indices and novel algorithms for predicting green LAI of crop canopies: modeling and validation in the context of precision agriculture. Remote Sens Environ. 2004;90(3):337–52. https://doi.org/10.1016/j.rse.2003.12.013
59. Gitelson AA, Zur Y, Chivkunova OB, Merzlyak MN. Assessing carotenoid content in plant leaves with reflectance spectroscopy. Photochem Photobiol. 2002;75(3):272–81.
60. Metternicht G. Vegetation indices derived from high-resolution airborne videography for precision crop management. Int J Remote Sens. 2003;24(14):2855–77. https://doi.org/10.1080/01431160210163074
61. Nguyen C, Sagan V, Maimaitiyiming M, Maimaitijiang M, Bhadra S, Kwasniewski MT. Early detection of plant viral disease using hyperspectral imaging and deep learning. Sensors.2021;21(3):742. https://doi.org/10.3390/s21030742
62. Chen JM. Evaluation of vegetation indices and a modified simple ratio for boreal applications. Can J Remote Sens. 1996;22(3):229–42.
63. Filella I, Serrano L, Serra J, Penuelas J. Evaluating wheat nitrogen status with canopy reflectance indices and discriminant analysis. Crop Sci. 1995;35(5):1400–5. https://doi.org/10.2135/cropsci1995.0011183X003500050023x

© The Author(s) 2026. Creative Commons CC BY 4.0. Published by Horizon e-Publishing Group.
https://doi.org/10.14719/pst.17031

64. Huang W, Guan Q, Luo J, Zhang J, Zhao J, Liang D, et al. New optimized spectral indices for identifying and monitoring winter wheat diseases. IEEE J Sel Top Appl Earth Obs Remote Sens. 2014;7(6):2516–24. https://doi.org/10.1109/JSTARS.2013.2294961
65. Chen T, Zhang J, Chen Y, Wan S, Zhang L. Detection of peanut leaf spots disease using canopy hyperspectral reflectance. Comput Electron Agric. 2019;156:677–83. https://doi.org/10.1016/j.compag.2018.12.036
66. Abdulridha J, Ampatzidis Y, Roberts P, Kakarla SC. Detecting powdery mildew disease in squash at different stages using UAV-based hyperspectral imaging and artificial intelligence. Biosyst Eng. 2020;197:135–48. https://doi.org/10.1016/j.biosystemseng.2020.07.001
67. Chappelle EW, Kim MS, McMurtrey JE III. Ratio analysis of reflectance spectra (RARS): an algorithm for the remote estimation of the concentrations of chlorophyll a, chlorophyll b and carotenoids in soybean leaves. Remote Sens Environ. 1992;39(3):239–47. https://doi.org/10.1016/0034-4257(92)90089-3
68. Blackburn GA. Spectral indices for estimating photosynthetic pigment concentrations: a test using senescent tree leaves. Int J Remote Sens. 1998;19(4):657–75. https://doi.org/10.1080/014311698215919
69. Bauriegel E, Giebel A, Herppich WB. Hyperspectral and chlorophyll fluorescence imaging to analyse the impact of *Fusarium culmorum* on the photosynthetic integrity of infected wheat ears. Sensors. 2011;11(4):3765–79.
70. Melgani F, Bruzzone L. Classification of hyperspectral remote sensing images with support vector machines. IEEE Trans Geosci Remote Sens. 2004;42(8):1778–90. https://doi.org/10.1109/TGRS.2004.831865
71. Rumpf T, Mahlein AK, Steiner U, Oerke EC, Dehne HW, Plümer L. Early detection and classification of plant diseases with support vector machines based on hyperspectral reflectance. Comput Electron Agric. 2010;74(1):91–9. https://doi.org/10.1016/j.compag.2010.06.009
72. Shuaibu M, Lee WS, Schueller J, Gader P, Hong YK, Kim S. Unsupervised hyperspectral band selection for apple Marssonina blotch detection. Comput Electron Agric. 2018;148:45–53. https://doi.org/10.1016/j.compag.2017.09.038
73. Karim A, Jumani TA, Raza MA, Baloch SK, Soomro NQ, Masud M, et al. Integration of deep learning and machine learning techniques for advancing the detection of plant diseases. Eng Rep. 2025;7(6):e70206. https://doi.org/10.1002/eng2.70206
74. Sankaran S, Ehsani R, Inch SA, Ploetz RC. Evaluation of visible-near infrared reflectance spectra of avocado leaves as a non-destructive sensing tool for detection of laurel wilt. Plant Dis. 2012;96(11):1683–9. https://doi.org/10.1094/PDIS-01-12-0030-RE
75. Zhao Y-R, Li X, Yu K-Q, Cheng F, He Y. Hyperspectral imaging for determining pigment contents in cucumber leaves in response to angular leaf spot disease. Sci Rep. 2016;6(1):27790. https://doi.org/10.1038/srep27790
76. Ashourloo D, Aghighi H, Matkan AA, Mobasheri MR, Rad AM. An investigation into machine learning regression techniques for the leaf rust disease detection using hyperspectral measurement. IEEE J Sel Top Appl Earth Obs Remote Sens. 2016;9(9):4344–51. https://doi.org/10.1109/JSTARS.2016.2575360
77. Villa A, Chanussot J, Benediktsson JA, Jutten C, Dambreville R. Unsupervised methods for the classification of hyperspectral images with low spatial resolution. Pattern Recognit.2013;46(6):1556–68. https://doi.org/10.1016/j.patcog.2012.10.030
78. Kuska M, Wahabzada M, Leucker M, Dehne H-W, Kersting K, Oerke E-C, et al. Hyperspectral phenotyping on the microscopic scale: towards automated characterization of plant-pathogen interactions. Plant Methods. 2015;11(1):28. https://doi.org/10.1186/s13007-015-0073-7
79. Polk SL, Chan AH, Cui K, Plemmons RJ, Coomes DA, Murphy JM, editors. Unsupervised detection of ash dieback disease (*Hymenoscyphus fraxineus*) using diffusion-based hyperspectral image clustering. IGARSS 2022–2022 IEEE International Geoscience and Remote Sensing Symposium; 2022. https://doi.org/10.1109/IGARSS46834.2022.9883429
80. Zhu H, Chu B, Zhang C, Liu F, Jiang L, He Y. Hyperspectral imaging for presymptomatic detection of tobacco disease with successive projections algorithm and machine-learning classifiers. Sci Rep. 2017;7(1):4125. https://doi.org/10.1038/s41598-017-04501-2
81. Baranowski P, Jedryczka M, Mazurek W, Babula-Skowronska D, Siedliska A, Kaczmarek J. Hyperspectral and thermal imaging of oilseed rape (*Brassica napus*) response to fungal species of the genus *Alternaria*. PLoS ONE.2015;10. https://doi.org/10.1371/journal.pone.0122913
82. Moshou D, Bravo C, Oberti R, West J, Ramon H, Vougioukas S, et al. Intelligent multi-sensor system for the detection and treatment of fungal diseases in arable crops. Biosyst Eng. 2011;108(4):311–21. https://doi.org/10.1016/j.biosystemseng.2011.01.003
83. Nagasubramanian K, Jones S, Singh AK, Sarkar S, Singh A, Ganapathysubramanian B. Plant disease identification using explainable 3D deep learning on hyperspectral images. Plant Methods. 2019;15(1):98. https://doi.org/10.1186/s13007-019-0479-8
84. Simonyan K, Vedaldi A, Zisserman A. Deep inside convolutional networks: visualising image classification models and saliency maps. arXiv preprint arXiv:13126034. 2013.
85. Wang D, Vinson R, Holmes M, Seibel G, Bechar A, Nof S, et al. Early detection of tomato spotted wilt virus by hyperspectral imaging and outlier removal auxiliary classifier generative adversarial nets (OR-AC-GAN). Sci Rep. 2019;9(1):4377. https://doi.org/10.1038/s41598-019-40066-y
86. Mahlein A-K, Alisaac E, Al Masri A, Behmann J, Dehne H-W, Oerke E-C. Comparison and combination of thermal, fluorescence and hyperspectral imaging for monitoring fusarium head blight of wheat on spikelet scale. Sensors. 2019;19(10):2281. https://doi.org/10.3390/s19102281
87. Abdulridha J, Ampatzidis Y, Kakarla SC, Roberts P. Detection of target spot and bacterial spot diseases in tomato using UAV-based and benchtop-based hyperspectral imaging techniques. Precis Agric. 2020;21(5):955–78. https://doi.org/10.1007/s11119-019-09703-4
88. Zhang J-C, Pu R-L, Wang J-H, Huang W-J, Yuan L, Luo J-H. Detecting powdery mildew of winter wheat using leaf level hyperspectral measurements. Comput Electron Agric. 2012;85:13–23. https://doi.org/10.1016/j.compag.2012.03.006
89. Leucker M, Mahlein A-K, Steiner U, Oerke E-C. Improvement of lesion phenotyping in *Cercospora beticola*–sugar beet interaction by hyperspectral imaging. Phytopathology.2016;106(2):177–84. https://doi.org/10.1094/PHYTO-04-15-0100-R
90. Yu R, Luo Y, Zhou Q, Zhang X, Wu D, Ren L. A machine learning algorithm to detect pine wilt disease using UAV-based hyperspectral imagery and LiDAR data at the tree level. Int J Appl Earth Obs and Geoinf. 2021;101:102363. https://doi.org/10.1016/j.jag.2021.102363
91. Hornero A, Zarco-Tejada PJ, Quero JL, North PR, Ruiz-Gómez FJ, Sánchez-Cuesta R, et al. Modelling hyperspectral- and thermal-based plant traits for the early

© The Author(s) 2026. Creative Commons CC BY 4.0. Published by Horizon e-Publishing Group.
https://doi.org/10.14719/pst.17031

detection of *Phytophthora*-induced symptoms in oak decline. Remote Sens Environ. 2021;263:112570. https://doi.org/10.1016/j.rse.2021.112570

92. Poblete T, Navas-Cortes JA, Hornero A, Camino C, Calderon R, Hernández-Clemente R, et al. Detection of symptoms induced by vascular plant pathogens in tree crops using high-resolution satellite data: modelling and assessment with airborne hyperspectral imagery. Remote Sensing of Environment. 2023;295:113698. https://doi.org/10.1016/j.rse.2023.113698
93. Feng Z, Song L, Duan J, He L, Zhang Y, Wei Y, et al. Monitoring wheat powdery mildew based on hyperspectral, thermal infrared and RGB image data fusion. Sensors. 2021;22(1):31. https://doi.org/10.3390/s22010031
94. Guo W, Rage UK, Ninomiya S. Illumination invariant segmentation of vegetation for time series wheat images based on decision tree model. Comput Electron Agric .2013;96:58–66. https://doi.org/10.1016/j.compag.2013.04.010
95. Yu K, Kirchgessner N, Grieder C, Walter A, Hund A. An image analysis pipeline for automated classification of imaging light conditions and for quantification of wheat canopy cover time series in field phenotyping. Plant Methods. 2017;13(1):15. https://doi.org/10.1186/s13007-017-0168-4
96. Liu Z-Y, Wu H-F, Huang J-F. Application of neural networks to discriminate fungal infection levels in rice panicles using hyperspectral reflectance and principal components analysis. Comput Electron Agric. 2010;72(2):99–106. https://doi.org/10.1016/j.compag.2010.03.003
97. Mahlein A-K, Kuska MT, Thomas S, Wahabzada M, Behmann J, Rascher U, et al. Quantitative and qualitative phenotyping of disease resistance of crops by hyperspectral sensors: seamless interlocking of phytopathology, sensors and machine learning is needed! Curr Opin Plant Biol. 2019;50:156–62. https://doi.org/10.1016/j.pbi.2019.06.007
98. Nagaraju M, Chawla P. Systematic review of deep learning techniques in plant disease detection. Int J Syst Assur Eng Manag. 2020;11(3):547–60. https://doi.org/10.1007/s13198-020-00972-1
99. Shafay M, Hassan T, Owais M, Hussain I, Khawaja SG, Seneviratne L, et al. Recent advances in plant disease detection: challenges and opportunities. Plant Methods. 2025;21(1):140. https://doi.org/10.1186/s13007-025-01450-0
100. Ferreira LdC, Carvalho ICB, Jorge LAdC, Quezado-Duval AM, Rossato M. Hyperspectral imaging for the detection of plant pathogens in seeds: recent developments and challenges. Front Plant Sci. 2024;15:1387925. https://doi.org/10.3389/fpls.2024.1387925

Additional information

Peer review: Publisher thanks the Sectional Editor and anonymous reviewers for their contribution to the peer review of this work.

Reprints & permissions information: Available at https://horizonepublishing.com/journals/index.php/PST/open_access_policy.

Publisher's Note: Horizon e-Publishing Group remains neutral with regard to jurisdictional claims in published maps and institutional affiliations.

Indexing: See https://horizonepublishing.com/journals/index.php/PST/indexing_abstracting.

Copyright: © The Author(s). This is an open-access article distributed under the Creative Commons Attribution License CC BY 4.0.

Publisher information: Plant Science Today is published by Horizon e-Publishing Group with support from Empirion Publishers Private Limited, Thiruvananthapuram, India.

© The Author(s) 2026. Creative Commons CC BY 4.0. Published by Horizon e-Publishing Group.

https://doi.org/10.14719/pst.17031